Dear Editor,

Herewith we submit the revised manuscript. First we would like to thank you and Dr Remer, two other reviewers, and Dr Korkin, and appreciate all the comments and suggestions. We have considered all of them and made changes accordingly in the revised paper.

In the following we will give our responses to the comments. To make the changes easier to identify, we have marked them with different colors.

Kind regards,
Guangliang Fu and Otto Hasekamp,
on behalf of all co-authors

(The revised manuscript is in the latter part of this pdf.)

Responses – part 1 (Reviewer 1):

Reply to comments:

1. *General comment. I understand that one of the purposes of this work is to determine expected uncertainty on the retrievals for the polarimeters. But AERONET and HSRL should already have documented expected uncertainty. It certainly would be helpful to indicate on the figures what is the expected uncertainty of the known sensors. We see values for MAE, bias, etc., but do not know how to put these values into context. If we knew AERONET uncertainty for that parameter, for example, context could be established.*

   Response:
   We agree. We added a phrase to the paper with respect to the expected AERONET AOD uncertainty in Sect. 3.5:
   " The uncertainty on AERONET AOD is 0.01 for mid-visible wavelengths and 0.03 for UV wavelengths (Eck et al., 1999) and is dominated by a calibration (systematic) error. "

   For the expected uncertainty in HSRL-2, we refer to the comparison between HSRL-2 and AERONET. We added the phrase in Sect. 4.2.1: " The bias between HSRL-2 and AERONET is within the AERONET uncertainty. The random differences, with standard deviation 0.029 at 380 nm and 0.014 at 532 nm are most likely due to HSRL-2 uncertainties. "

2. *General comment. This is a corollary to (1). AERONET AOD has very small uncertainty, but AERONET retrieved products and these include the SDA products have larger error bars. The goal in comparing polarimeter retrievals to these other retrievals is comparison, not validation. This was not explicitly stated in the paper.*

   Response:
   We agree and explicitly state this to the paper in Sect. 3.5:
   " The multispectral aerosol optical depth (AOD) from the MAP and lidar retrievals is validated with AERONET (AErosol RObotic NETwork) level 1.5 data (Holben et al., 2001) (version 3.0). The data are cloud cleared. The uncertainty on AERONET AOD is 0.01 for mid-visible wavelengths and 0.03 for UV wavelengths (Eck et al., 1999) and is dominated by a calibration (systematic) error. The effective radius for fine and coarse modes are

compared with AERONET level 1.5 Almucantar Retrieval Inversion Products (Dubovik et al., 2002). The AOD of fine and coarse modes are compared with AERONET level 1.5 spectral de-convolution algorithm (SDA) data (O'Neill et al., 2003). It should be noted that the inversion- and SDA products are quite uncertain themselves at low AOD so the comparison to these products should not be considered a validation. "

3. *General comment. I see in the description of the different data sets mitigating strategies for inhomogeneity for registering the different angular views. Does this include topographical variation?*

Response:
Yes, this does include topographical variation.

4. *Page 9. Last paragraph that begins with "As with the extinction products", I'm a little unclear on what is being said here. "HSRL method" is when HSRL measures extinction. "assumed lidar ratio" is when it does not. The HSRL method is not available in many situations during ACEPOL, so the lidar information is going to come to us like an old-fashioned backscattering lidar with an assumed lidar ratio. It's not clear why the HSRL method is going to be unavailable. Then here it seems to imply that there is going to be a choice between the two methods, not that the HSRL method is unavailable, but that both are available. And then it says that the assumed lidar ratio method is actually BETTER than the HSRL method at low loading. This is because one measures its uncertainty in a relative sense and the other in an absolute sense. The fact that the assumed lidar ratio can be better than the HSRL method is very strange to me. Did I understand this paragraph correctly?*

Response:
Thanks for pointing out this point. Actually the statement "For ACEPOL, the extinction, AOD, and lidar ratio from the HSRL methodology are not available for many ground pixels." was not accurate (which was based on the old version HSRL-2 data). We have removed this statement and re-wrote that part to avoid confusion in Sect. 3.4: " For ACEPOL, the extinction products from the HSRL method are reported at 150 m vertical resolution and at temporal resolution of 60 s generally and 10 s. Additionally, the aerosol extinction products at 355 nm and 532 nm are also provided based on the aerosol backscatter and an assumed lidar ratio of 40 sr, and reported at the backscatter resolution.

Similarly, the AOD is reported from the standard HSRL approach and also the AOD calculated using assumed lidar ratio is provided. "

Yes, we have two AOD products as two choices. For the low AOD case the AOD from the assumed lidar ratio is better than the HSRL method. This is because for low AOD,

both approaches are difficult, but the AOD from the assumed lidar ratio is expected to be smaller (given that the AOD is small) than the systematic uncertainty ∼0.05 from the HSRL method for ACEPOL.

5. *Section 3.5. AERONET section. Level 1.5 is cloud cleared, but not quality controlled. Also be aware that fine and coarse as defined by both the almucantar retrievals and the SDA methods are going to be different than defining fine and coarse by specific modes as is done in the polarimeter retrieval (Table 1). This may introduce differences in your comparisons. It did with the MODIS Dark Target over ocean retrieval.*

Response:
Thanks. We added this point to the paper in Sect. 4.1:
" Also, it should be noted that the "fine" and "coarse" as defined by the Almucantar retrievals are different with defining "fine" and "coarse" by specific modes as shown in Table 1. This may introduce differences in the comparisons. "

6. *Page 11-12. Discussion of comparison of effective radius against AERONET. Perhaps AERONET is wrong here? This is retrieval vs. retrieval, not retrieval vs. truth. And the loading is extremely low. I would think that everybody is running on fumes here. This applies to fine mode, but especially to coarse mode. Nobody has SWIR to really nail coarse mode. And AERONET's definition of fine and coarse modes, and their respective effective radii, are defined differently than the five modes in Table 1.*

Response:
We agree and included this aspect to the paper in Sect. 4.1:
" It is important to note that for the low AOD values encountered during ACEPOL, the AERONET retrieved fine and coarse mode AOD and effective radius are very uncertain themselves. Therefore, this comparison should not be interprested as "retrieval versus truth" but rather as "retrieval versus retrieval". "

7. *Figure 3. If I'm interpreting these plots correctly... The MAP retrievals can be very different from AERONET. For example, RSP has differences of -0.04 where the (AERONET + RSP)/2 = 0.025. This means that RSP retrieved tau_c of 0.005 and AERONET 0.045. In absolute terms that's not a lot, but in terms of relative contributions of the coarse mode to the total AOD it is a lot. Is it within expected error of the AERONET retrieval? It would be very helpful to have some context for the magnitude of the differences.*

Response:

We added some context for the magnitude to the paper in Sect. 4.1:
" The comparison shows a MAE of 0.028, 0.029, and 0.012 for SPEX, RSP, and airMSPI, respectively for τ^{f} and 0.026, 0.028, 0.017 for τ^{c}. The bias is 0.028, 0.019 and 0.004 for τ^{f} and 0.025, 0.028, and 0.003 for τ^{c}. So, SPEX and RSP have an overestimation of the fine mode and an underestimation of the coarse mode, compared to AERONET SDA product. Although these biases are large in a relative sense (given the low AOD, especially for the coarse mode), they are within the expected error from the AERONET SDA product. AirMSPI compares better to the AERONET SDA product than SPEX airborne and RSP. "

8. *Section 4.2.1 These comparisons are all with "assumed lidar ratio". Are these the only days with collocations? If there is a choice between assumed lidar ratio and HSRL method, how does the HSRL method compare?*

Response:
Indeed all HSRL2-AERONET collocations are included. We have explicitly mentioned in Sect 3.4, the comparisons in Figure 4 are with the assumed lidar ratio. For these low AOD cases, the comparison against AERONET for HSRL AOD from the HSRL method is worse than from the assumed lidar ratio. The reason has been explained in Sect 3.4.

9. *Section 4.2.2. I grew up in Los Angeles and the Central Valley, so I know this territory well, but not everybody does. Maybe use "east" and "west" without place names, or annotate the image.*

Response:
Thanks. We changed them to the paper in Sect. 4.2.2:
" From this figure it follows that there were very low AOD values for the eastern part of the scene and somewhat higher values in the western and south-western part of the scene. "

10. *Final sentence of Section 4.2.2. "The differences from the direct comparison between SPEX and RSP are somewhat larger than those from individual comparisons with HSRL-2 of SPEX and RSP, respectively. This suggests that the differences with HSRL-2 are not caused by common assumptions in the SPEX and RSP retrievals, but are rather caused by errors that are specific to each MAP". I don't follow the logic.*

Response:
If the differences with HSRL-2 are caused by common assumptions in the SPEX and RSP retrievals, the differences should be smaller when comparing SPEX and RSP (than compar-

ing MAPs with HSRL-2) because the common assumptions should have little effect when comparing SPEX and RSP. However, the comparison between SPEX and RSP is worse than comparing MAPs with HSRL-2. Thus, we reach the statement " This suggests that the differences with HSRL-2 are not caused by common assumptions in the SPEX and RSP retrievals, but are rather caused by errors that are specific to each MAP"

11. *Section 4.2.3. page 13. Lines 15-17. "It should be noted that the smoke plume exhibits large spatial variation so part of the MAP-lidar differences can be attributed to the fact that different instruments see a slightly different part of the smoke plume". What about different angles from the same instrument seeing different parts of the smoke, or what if the smoke changes between the fore and aft angles are measured? What happens to the retrieval? It would be really nice to have a quantitative sense of how variable that plume is. Could we see a spatial plot of the smoke retrievals or at least have stdev on the parameters shown in Table 2.*

Response:

If the different viewing angles would see different parts of the smoke plume, this would result in a large χ^2 of differences between forward model and measurements. This is not the case for the points in the Figure 7.

To illustrate the spatial variability of the smoke plume, we have included Figure 7a, which gives a sense of how variable the AOD of smoke plume is. We have also included the standard deviation inside the plume from SPEX and RSP on the parameters shown in the Table 3.

12. *Page 13. Lines 25-26. "Our explanation for this, is that at high AOD the measured radiance and DoLP are less affected by the co-registration errors between viewing angles than for low AOD". How could this be? The evolving, hetereogeneous smoke plume has to be more difficult to co-register between angles than the unmoving ground.*

Response:

The land surface can be very patchy, especially near Fresno and Bakersfield. This leads to higher spatial variability in the radiance than the spatial variation of the smoke plume at 100 meter scale. The difference in co-location between the MAPs and HSRL-2 sampling may however be 1 km.

13. *Page 13. Lines 33-34. On the other hand, I think this is a really good explanation: "A possible explanation for the difference could be the simplified description of non- spherical*

particles in our retrieval approach. "

Response:
Thanks.

14. *Figure 7d-f. Are lidar ratios here retrieved via HSRL method, or assumed? If assumed, does these figures make any sense. If retrieved, then why not use retrieved throughout the paper? Or show that they are worse than assumed. This whole retrieved vs. assumed lidar ratio choice never sat well with me throughout the manuscript.*

Response:
Shown in the plots are those retrieved from the HSRL method. This is consistent with our comparison for the smoke case for high AOD from the HSRL method. The only place we use the assumed lidar ratio is for the comparison of AOD in the low AOD case. For these cases we do not compare the lidar ratio because indeed that would not make sense.

15. *Table 2. Maybe show stdev along with mean? Or show spatial distribution if any of these properties are varying downwind?*

Response:
We have done so in the revised manuscript. Please see Figure 7a and Table 3.

16. *Page 14. Line 13. "the latter value is closer to the ALH derived from HSRL-2 (2.64 km)". Sure slightly closer, but still 1 km off. Not that much different from SPEX.*

Response:
We agree. We re-wrote the phrase to the paper in Sect. 4.2.4:
" For the Aerosol Layer Height (ALH), SPEX retrieves a higher value (4.417 km) than RSP (1.148 km), where the latter value is somewhat closer to the ALH derived from HSRL-2 (2.64 km). "

17. *Page 14. Line 14. The explanation of ALH being difficult to retrieve without UV might be elaborated on a little here.*

Response:
We added a phrase to the paper in Sect. 4.2.4:

" Here, it should be noted that for SPEX the shortest wavelength that is used in the retrieval is 450 nm, so we do not expect an accurate ALH retrieval because the retrieval of ALH from polarization requires a strong signal from Rayleigh scattering (Wu et al., 2016). "

18. *Finally. . . don't you want to state a conclusion? What is the overarching thing you have learned? If this were my paper I would conclude that the 3 polarimeters are producing comparable results when forced through the same algorithm. The exception being aerosol layer height and perhaps some coarse mode parameters, which suffer from not having the bands that these parameters are sensitive to: shortwave (410 nm) and SWIR, respectively. So when there is no sensitivity, the retrieval becomes a random number generator. But for parameters that the instruments are sensitive to, there is little difference between instruments. It is still TBD whether algorithmic differences are going to matter. But it is not my paper. The authors can choose to write a conclusion of their choice. Or not.*

Response:

Thanks. We included these summaries to the paper in the conclusion part:

" In this study, 3 polarimeters produced comparable results when using the same algorithm. The exception were the ALH and some coarse mode parameters, which were mainly caused by not having the bands that these parameters were sensitive to: shortwave (410 nm) and SWIR, respectively. For parameters that the instruments were sensitive to, good agreements were found among instruments. Our results corroborate the findings of earlier studies that different combinations of spectral and angular measurements yield a very similar retrieval capability for aerosol properties (Hasekamp and Landgraf, 2007; Wu et al., 2015; Hasekamp et al., 2019) "

Responses – part 2 (Reviewer 2):

Reply to General comments:

1. *When the authors introduce the SRON multimode retrieval algorithm in section 2.1, no aerosol size distribution parameters are included in the state vector. However, in the retrieval results, effective radius of fine and coarse mode particles are shown. Although the calculation of fine and coarse mode effective radius is presented in section 2.2, the retrieved aerosol parameters related to size parameters are not clear.*

   Response:
   Thanks. We added a description of the multimode retrieval algorithm to the paper in Sect. 2.1:
   " In principle, the idea of the multimode approach is that instead of fitting the size distribution parameters (the effective radius r_{eff} and the effective variance v_{eff}) of two modes, one aims to fit the size distribution with a larger number of modes for which r_{eff} and v_{eff} are fixed. The advantage of this approach is that it makes the inversion problem more linear since r_{eff} and v_{eff} tend to make the inversion highly nonlinear. Another advantage is that the multimode approach has more freedom in fitting different shapes of size distribution if the number of chosen modes is sufficiently large. In this paper, multimode retrievals based on 5 modes are used and the aerosol size distribution are described in Table 3 (Fu and Hasekamp, 2018). "

   In the retrieval, we don't retrieve r_{eff} and v_{eff} for the 5 modes. The fine and coarse effective radius are calculated after retrievals based on Sect. 2.2. The sensitivities of the retrieved aerosol parameters related to different particle size parameters (parametric 2-mode, 3 to 10 multimode) have been extensively studied in Fu and Hasekamp (2018).

2. *As defined in the manuscript, the χ^2 used to decide retrieval convergence is different for different instruments. For example, for AirMSPI, observed intensities in 8 bands and DoLP in 3 bands are used in the retrieval, while radiance and DoLP at 16 wavelengths for SPEX are used. Although χ^2 is defined as a mean value of total number of measurements, the ratios ($\frac{F_i - y_i}{S_y(i,i)}$) in Eq. 3 for radiance and DoLP may have different scales. Therefore, if different numbers of radiances and DoLP are used even though two instruments have the same total number of measurements, the χ^2 may differ a lot. Does this problem affect the retrieval results between different instruments? Do they use the same threshold χ^2_{max}?*

Response:
In this paper, for different instruments we use the same threshold $\chi^2_{\max} = 1.5$. It is true that for the different instruments there are different contributions to the χ^2. This would only pose a problem if the assumed errors in S_y are a poor representation of the true measurement errors. We believe we have used reasonable error estimates in our S_y for the differnt instruments so this should not pose a problem.

3. *The retrieval results of 3 different instruments are compared in this manuscript, but only some statistical parameters, such as MAE, bias and STD are presented. Are there any conclusions or suggestions about the measurements (radiance or DoLP) at which wavelengths are combined better for aerosol retrieval? Or are different numbers of multi-angle measurements affect aerosol retrievals a lot? I think more similar common summaries could attract audiences.*

Response:
Our study confirms earlier studies that different combinations of spectral and angular measurements yield a very similar retrieval capability for aerosol properties (Hasekamp and Landgraf, 2007; Wu et al., 2015; Hasekamp et al., 2019). We have highlighted this in the conclusion of the revised manuscript.

4. *In the state vector, aerosol column numbers and microphysical properties are included, thus the AOD in the retrieval at different wavelengths are calculated from retrieved column numbers and other parameters. I'm a little confused that why the authors use different wavelengths when compare total AOD and fine and coarse modes AOD (Figure 1 and Figure 3). If the same wavelengths are used, the retrieval performance of fine, coarse mode AOD and total AOD can also be evaluated.*

Response:
Only measurements at 500 nm have been used to compare the fine and coarse mode AOD because the measurements (fine and coarse mode AOD) at other wavelengths are not available in the SDA product.

5. *The surface reflectance parameters are retrieved simultaneously with aerosol properties in the algorithm. How is the performance of surface reflectance retrieval in the campaign? Are the accuracies of retrieved aerosol properties related to surface reflectance?*

Response:

We do not have a good reference to evaluate the accuracy of the retrieved surface parameters. Instead, we have evaluated the difference between MAP and HSRL-2 as function of retrieved surface properties. The results are show in Figure R1 of this response. We do not see clear correlation with surface parameters here.

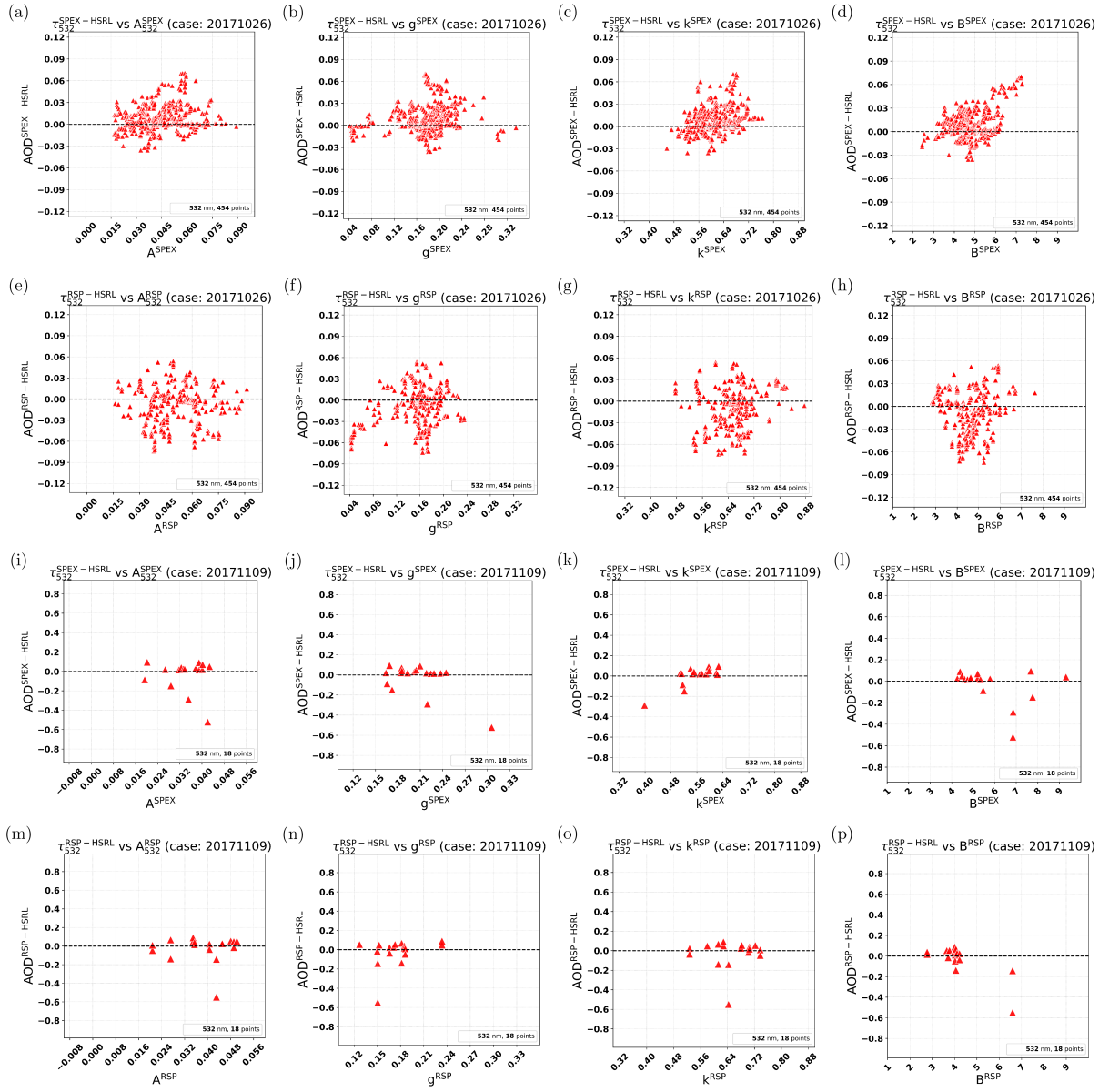

Figure 1: **Sensitivities between AOD differences (between MAPs and HSRL-2) and surface parameters. (a)-(h)** the low AOD case. **(i)-(p)** the high AOD (smoke) case. 1st, 2nd, 3rd, and 4th column respectively represent results with respect to BRDF scaling parameters for wavelength bands (A_{532}), Parameter 1 of RPV model (g), Parameter 2 of RPV model (k), and Scaling parameter for polarized reflectance (B).

6. *The retrieval accuracy of fine and coarse mode AOD depend on the retrieved aerosol microphysical properties. If the dependence of the retrieval bias of τ^f and τ^c on the accuracy of retrieved r_{eff} or refractive index is shown, it will be interesting and beneficial for distinguishing aerosol types.*

Response:
We do not see such dependencies in the available data and also we do not really expect it.

Reply to Specific comments:

1. *In the introduction part, the third paragraph in page 2 indicates that combining both intensity and polarization measurements at multiple viewing angles is beneficial for aerosol retrieval. However, this paragraph is too short and simple. This is the most important feature of 3 MAPs used in this manuscript to do retrieval. I think more theoretical foundation and how previous studies use these information could be added.*

Response:
We extended the paragraph 3 (in the introduction) in the paper by adding a review of previous studies:
" The reason is that the angular dependence of the scattering matrix elements related to linear polarization, depend strongly on the microphysical aerosol properties, like refractive index and particle size (Hansen and Travis, 1974; Mishchenko and Travis, 1997). Furthermore, the polarization signal is mostly dominated by light that has been scattered only once, which means that the characteristics of the scattering matrix remain largely preserved in a top-of-atmosphere polarization measurement. The added value of polarization has been demonstrated by a number of studies on synthetic measurements (Mishchenko and Travis, 1997; Hasekamp and Landgraf, 2007; Hasekamp, 2010; Knobelspiesse et al., 2012), airborne measurements (Chowdhary et al., 2005; Waquet et al., 2009; Xu et al., 2017; Wu et al., 2015, 2016), and spaceborne measurements (Hasekamp et al., 2011; Dubovik et al., 2011; Fu and Hasekamp, 2018). These algorithms can be divided in two main groups: LookUp-Table (LUT) based approaches and full inversion approaches. Generally speaking, LUT approaches are faster but less accurate than full inversion approaches because LUT approaches choose the best fitting aerosol model from a discrete lookup table. Full inversion approaches are more accurate but slower because they require radiative transfer calculations as part of the retrieval procedure. The LUT algorithms are e.g., the LOA LUT algorithm over ocean (Deuzé et al., 2000), the LOA LUT algorithm over land (Deuzé et al., 2001; Herman et al., 1997), and the SSA LUT algorithm (Waquet et al., 2016). The full inversion algorithms are e.g., the GRASP algorithm (Dubovik et al., 2011), the SRON-Aerosol algorithm (Hasekamp and Landgraf, 2007; Hasekamp et al., 2011; Stap et al., 2015;

Wu et al., 2015, 2016; Di Noia et al., 2017; Fu and Hasekamp, 2018), the JPL algorithm (Xu et al., 2017), the GISS algorithm (Waquet et al., 2009) and the MAPP algorithm (Stamnes et al., 2018). Besides, some additional aerosol retrieval approaches can be found in (Sano et al., 2006; Cheng et al., 2011; Masuda et al., 2000; Lebsock et al., 2007). It should be noted that of the full inversion approaches only the SRON-Aerosol algorithm and the GRASP algorithm have been applied at a global scale. "

We also included more theoretical description for the retrieval algorithm in Sect. 2.1 from Eq. (4) to (6).

2. *The paragraph at page 3 line 6-10 has little relationship with this study. I believe the authors could delete or short this paragraph and combine it with last paragraph.*

Response:
Thanks. We have shorted this paragraph and combined it with the previous paragraph, as stated in the end of paragraph 4 of introduction:
" The POLDER design also forms the blueprint for the 3MI instruments (Fougnie et al., 2018), to be flown on METOP-SG in the time frame ∼2020-2035. "

3. *When giving the information of ACEPOL campaign in the introduction, the information about the altitude aircraft flying is suggested to be provided due to the retrieval of ALH, especially at smoke plume case whose ALH is always high.*

Response:
We agree. We added the altitude of the NASA ER-2 flight in the introduction: " All 4 airborne MAPs listed above were mounted on the NASA Earth Resources-2 (ER-2) high altitude (∼20 km) aircraft (Navarro, 2007) during the Aerosol Characterization from Polarimeter and Lidar (ACEPOL) campaign, which was performed from October-November 2017, starting from the NASA Armstrong airbase in Palmdale, California. "

4. *At page 4 line 20, the meaning of k in the equation is not explained.*

Response:
Thanks. We added it to the paper in Sect. 2.1:
" where k is a parameter that varies between 0 and 1. This parameter controls the slope of the reflectance with respect to the illumination and view angles (Rahman et al., 1993). "

5. *At page 11 line 18-19, the authors present "the MAE gets smaller with increasing wavelengths, which is mainly caused by the fact that AOD value itself decreases with wavelength". Some other parameters such as mean relative error (MRE) or root mean squire error (RMSE) could remove this effect and are recommended to be compared.*

   Response:
   Thanks. Yes, the MRE can remove this effect, but the RMSE not. We added the MRE to the paper for all the AOD comparisons with AERONET and HSRL-2, and indeed see that the MRE does not decrease with wavelength.

6. *The sentences at line 22-23 and line 30-31 in page 11 present the same thing.*

   Response:
   We re-wrote the latter one (which is especially for the coarse mode effective radius) to the paper in Sect. 4.1:
   " This is in line with synthetic studies (e.g., Hasekamp et al. (2019)) that $r_{\text{eff}}^{\text{c}}$ is a difficult parameter to retrieve, in particular for small AOD values. "

7. *At page 13 line 1-2, "for low AOD the effect of the surface on the measured radiances is larger than for SPEX airborne" is presented. I'm a little confused why.*

   Response:
   We re-wrote this sentence to:
   " A possible explanation is that for low AOD the radiance and polarization measurements have strong influence from the spatially inhomogeneous surface, and therefore errors due to inter-angle mis-registration, which are larger for RSP than for SPEX, may be significant. "

8. *At page 14 line 13-14, the authors explained that the shortest wavelength for SPEX is 450 nm and not suitable for ALH retrieval. Do you mean the shorter wavelengths such as UV band benefit ALH retrieval? More clear and straight forward sentences are suggested to be used. Moreover, this explanation for ALH retrieval is too simple and this may be only one of many reasons. I believe reading more related papers about ALH retrieval could help the authors explain this problem more clearly and deeply.*

   Response:
   To our best knowledge, Wu et al. (2016) is the only paper for ALH retrieval from MAP measurements. We extended the explanation in Sect. 4.2.4 by adding:

" Here, it should be noted that for SPEX the shortest wavelength that is used in the retrieval is 450 nm, so we do not expect an accurate ALH retrieval because the retrieval of ALH from polarization requires a strong signal from Rayleigh scattering (Wu et al., 2016). "

9. *Some sentences in this manuscript are a little complex and confused, especially in section 1 and section 4. More concise sentences are recommended.*

Response:

Thanks. We believe both Section 1 and 4 have been improved in the new version paper.

Responses – part 3 (Reviewer 3):

Reply to General comments:

1. *Although the paper focuses on aerosol retrievals, surface is an important component in the retrieval process and is included in the state vector. A good characterization of surface reflectance can significantly affect the retrieval accuracy of aerosol properties, which is especially true when aerosol loading is small (such as of the most ACEPOL cases). So, as a reader I would like to see some retrieval results for surface BRDF/BPDF properties and how the retrievals behave between different polarimeters.*

   Response:
   Thanks. We included a figure (Figure 6) showing the dependence of AOD difference between MAP and HSRL2 as function of the surface reflection (A) at 532 nm in the revised manuscript.

2. *The retrieval algorithm needs some more clarification in a few aspects of the radiative transfer calculations and the inversion configurations. These include: (i) which radiative transfer model and what are the relevant assumptions (such gas absorptions, Rayleigh scatterings, etc) in the radiative transfer assumptions? (ii) How the first guess of the state vector is defined? While the first guesses for aerosol parameters are mostly given, the paper mentions nothing about prior values for surface BRDF/BPDF parameters. (iii) It is not clear how the aerosol refractive index are treated, although it is mentioned to use the D'Almeida et al (1991) database. (iv) It is also not clear about how the weighting matrix (W) in the cost function is defined, as well as the threshold for the goodness of fit. Please refer to the relevant specific comments below for more details.*

   Response:
   - (i) We use the SRON radiative transfer mode LINTRAN (Hasekamp and Landgraf, 2005; Schepers et al., 2014). Rayleigh scattering cross sections are from Bucholtz (1995). Values for O3, NO2, and H2O columns are taken from MERRA-2 and AFGL as mentioned on page 11.
   -(ii) The first guess is obtained using a LUT approach. We extended the description. The LUT retrieval provides first guess values for aerosol and surface properties. The LUT retrieval itself starts with fixed values for all surface properties, i.e., 0.05, -0.09, 0.80, 1.0 for A, g, k, B, respectively. The prior values are listed in Table 2 of the revised manuscript.
   -(iii) The treatment of the refractive index is explained end page 4 and start page 5. The

coefficients are included in the state vector.
-(iv) We include the values for the weighting matrix in Table 2 of the revise manuscript.

3. *By reading the title of the article (Aerosol retrievals from the ACEPOL campaign), I would expect to see aerosol retrievals from different polarimeters and from their respective aerosol products. Are there any aerosol products available from the ACEPOL campaign with other existing retrieval algorithms? If yes, it would be more helpful to compare the aerosol retrievals from different algorithms. Such a comparison may also explain the consistent biases in the retrieved aerosol size (Figure 2), depolarization ratio and lidar ratio (Figure 7). Otherwise, I would suggest to make the article title more specific, for instance, by adding "using the SRON algorithm".*

Response:
We agree maybe the title is too general, and we have changed the title to:
" Aerosol retrievals from different polarimeters during the ACEPOL campaign using a common retrieval algorithm "

Reply to specific comments:

1. *Page 4, first paragraph of section 2.1. Description about aerosol refractive index is too brief. Please clarify: (i) at which relative humidity (RH) is assumed for the D'Almeida et (1991) database, or a dynamic RH relationship is considered with ancillary meteorological data? This is important as the inorganic aerosols are strongly hygroscopic. (ii) How the coefficients are defined for combining the aerosol species? In terms of volume concentrations? (iii) Are the different aerosol species internally or externally mixed in the calculation of modal refractive index? In addition, it would be helpful if the refractive indices used in this study being provided in a supplemental document.*

Response:
(i) We only use the refractive index spectra from d'Almeida for the spectral dependendence of the refractive index. So. no assumtions are needed on RH.

For the comment (ii) we have added more description to the paper in Sect. 2.1:
" The coefficients α_k are the real numbers between 0 and 1, and are defined as weighting factors to combine the refractive index spectra for different aerosol components, e.g., DUST, water (H2O), Black Carbon (BC), INORGanic matter (INORG). In this study, we set $n_\alpha = 2$ and assume that spectral dependence of the fine mode and the coarse mode refractive indices can be described respectively by INORG+BC and DUST+INORG. Note that this assumption is flexible and can be updated according to the information content

of the measurement. Also spectra based on Principal Component Analysis (PCA) can be used as in Wu et al. (2015). The standard refractive index spectra are only used to describe the spectral dependence as the MAP measurements do not contain sufficient information to retrieve the refractive index for each wavelength separately. "

Comment (iii):
We compute the refractive index given the formula on top of page 5 of the revised manuscript. Given that we perform one Mie/T-matrix computation per mode for one refractive index, this implicitly assumes internal mixing.

2. *Page 5, line 6. Please give the explicit expression for R(G).*

Response:
In the new version, we included $R(G) = \frac{1-A(\lambda)}{1+G}$ in the Sect. 2.1.

3. *Section 2.1. The number of elements in state vector for different sensors would be different because of the different number of spectral bands. I would recommend include a table to list the detailed elements (and numbers) of the retrieved parameters for individual polarimeters. Correspondingly, the selected bands and number of angles for each observation set (as described in section 3.1-3.3) can also be listed in the same table. This will give the reader a clearer picture about the retrieval configuration for different sensors.*

Response:
Thanks. We have included Table 2 as suggested, which lists the viewing angles and wavelengths used in retrievals among SPEX airborne, RSP, and AirMSPI. The state vectors corresponding to these three polarimeters are also listed in the table. For the state vector, the only difference among three instruments is the BRDF scaling parameter $A(\lambda)$ which is wavelength-dependent.

4. *Section 2.1. It is not mentioned in algorithm description about: (i) what radiative transfer model is used and how many layers of atmosphere is assumed; (ii) how the gas absorption are treated; (iii) How the Rayleigh scattering are calculated. Please clarify.*

Response:
We have clarified these aspects in Sect. 2.1: " **F** consists of a radiative transfer model, for which we use the SRON radiative transfer model LINTRAN Landgraf et al. (2001); Hasekamp and Landgraf (2002, 2005); Schepers et al. (2014). All the radiative transfer

calculations are performed for a model atmosphere that includes Rayleigh scattering, scattering and absorption by aerosols, and gas absorption. Rayleigh scterring cross sections are used from Bucholtz (1995). The forward model simulates Stokes parameters I, Q, U at the top of the atmosphere (800 km) or the height of the research flight (e.g., ∼20 km for NASA ER-2 in this paper) for given optical properties (scattering and absorption optical thickness and scattering phase matrix for each vertical layer of the model atmosphere (15 layers of atmosphere is assumed). The other part of the forward model computes the optical properties from the aerosol microphysical properties using the tabulated kernels of Dubovik et al. (2006) for a mixture of spheroids and spheres. ”

5. *Page 5, Equation (2). Please clarify how the weight matrix (W) is defined to regulate the ranges of individual state parameters.*

Response:
Table 2 of the revised manuscript gives the elements of the weighting matrix. It has a comparable role as the prior covariance matrix in Optimal Estimation, except that for our inversion we have an additional regularization parameter that scales the whole matrix.

6. *Page 5, Equation (2). It is not clear how the prior state vector is defined for surface parameters. Please clarify.*

Response:
For the comment 5 and 6, we added a phrase to the paper in Sect. 2.1:
“ Table 2 shows the values in $\vec{x}_a$ including the prior values for aerosol and surface parameters. **W** is a diagonal matrix and its diagonal values are also shown in Table 2 (in the “weight” column). ”
Table 2 is included in the new version paper.

7. *Page 5, line 15. It is mentioned here “Stokes parameters I, Q, U at the top of the atmosphere” are simulated, but it is not clear what is the TOA altitude as defined. Moreover, the ACEPOL measurements are taken at an altitude of the ER-2 flights. The radiative transfer model should simulate the radiances as observed at the flight level. Please justify.*

Response:
Yes. We have added information to avoid confusion in Sect. 2.1:
“ The forward model simulates Stokes parameters I, Q, U at the height of the observation (e.g., ∼20 km for NASA ER-2 in this paper) ... ”

8. *Page 5, line 29. Is a constant threshold for Kai-Square used for all retrievals across different instruments? Please clarify.*

Response:
Yes, we use 1.5 as the threshold for all instruments and for all retrieval cases in the paper. This was already mentioned in the Sect. 4.

9. *Page 6, Equation (4). The symbol "G" is already used in equation (1) to denote hot-spot geometry factor. A different symbol should be used to avoid ambiguity.*

Response:
Thanks. We have used "O" to replace "G" here.

10. *Page 6, Equation (7). Are there any references for calculating the columnar depolarization ratio in this way? I recall some studies (sorry I couldn't find the paper) used layer extinction coefficient (rather than backscatter coefficient) as the weighting parameter.*

Response:
Actually, either the extinction coefficient or the backscatter coefficient can be taken as the weighting parameter. The reason why we use backscatter coefficient here is because for ACEPOL, the backscatter profiles from HSRL-2 are more accurate than the extinction profiles from HSRL-2.

11. *Page 9, line 24. Do you meant to "Where the HSRL method is NOT available for the extinction products . . .."*

Response:
We have changed that part in the new version to avoid confusion:
" For ACEPOL, the extinction products from the HSRL method are reported at 150 m vertical resolution and at temporal resolution of 60 s generally and 10 s. Additionally, the aerosol extinction products at 355 nm and 532 nm are also provided based on the aerosol backscatter and an assumed lidar ratio of 40 sr, and reported at the backscatter resolution. "

12. *Page 11, line 32. It seems the effective radius for coarse modes 4 and 5 are much smaller than the AERONET climatology as reported in Dubovik et al (2002). So why not define a large effective radius values for these two modes.*

Reference: Dubovik, O. et al (2002), Variability of Absorption and Optical Properties of Key Aerosol Types Observed in Worldwide Locations, Journal of the Atmospheric Sciences, 59(3), 590-608.

Response:

Yes, this is also possible. Actually we have other options for multimode retrievals as shown in Table 2 of Fu and Hasekamp (2018). For example, in the 7-mode retrieval, the largest effective radius is $3.0\,\mu m$. We can also re-define another 5 modes with larger effective radius for coarse modes 4 and 5. But for the 5-mode retrieval used in this paper, given that all the parameters seem to be well retrieved except for the coarse mode AOD (biased with AERONET SDA data) which is very small for the ACEPOL campaign, we think the current 5 modes are still reliable for this study.

13. *Figure 28. Authors may consider to replace the background of Figure 28a with a true color image of the smoke plume. I have seen such a figure from AirHARP gallery. It would be even better if a retrieved AOD map for the smoke plume is presented here.*

Response:

For the true color image of the smoke plume, we don't have it. We included Figure 7a on SPEX spatial sampling, which gives a sense of how variable the smoke plume is. Figure 7a is the retrieved AOD map for the smoke plumn.

14. *Page 13, line 23-24. It is mentioned here the smoke plume has large spatial variability that may contribute to the retrieval uncertainty. The suggestion above (#13) would at least give a visual expression how large the spatial variability is. In addition, the MAP algorithm would have challenge to retrieve AOD as different view angles see different location (thus AOD) of the elevated plume due to the parallax displacement. Can the authors provide some insights on how to addressing this challenge in the retrieval?*

Response:

The different viewing angles see a slightly different location but the difference is on the order of 100 meter. We do not expect the AOD to vary drastically over this distance. The difference in sampling between the MAPs and HSRL-2 however, may be on the order of 1 km, which may affect the comparion, as AOD will show some variation over a distance of 1 km in the smoke plume. So, the variability is not so large that it affects the retrieval uncertainty but rather limits the comparison to HSRL2.

15. *Finally, I would like to see a figure of retrieved particle size distribution for the smoke case, which would help interpreting the retrieval results listed in Table 2.*

Response:

We agree, and have included Figure 9 in the paper for number particle size distribution from SPEX and RSP in the smoke plume.

Responses – part 4 (SC reviewer):

Reply to comments:

1. *The 'alpha * Rpol' part in Eq.(1), p.4, seems unclear to me. Please provide explicit form for the Rpol matrix like it is done for the RPV-part. Reference to the Maignan et al, 2009 paper gives little help:*
   1) Sections 3.2, 3.3, and 3.5 in Maignan et al. 2009 discuss different models - which particular one was used in the paper under review? 2) As far as i know, Maignan et al. 2009 does not define the Mueller matrix of the surface - only BPDF, which is based on the F12=F21=Fp element of the Fresnel matrix. To get the Mueller matrix, shall one compute matrix exponential of the Fresnel matrix, or, vice versa, create a matrix of "scalar" exponents of elements of the Fresnel matrix? 3) The complete 4x4 (or reduced 3x3 if V is ignored) Mueller matrix of the surface is required only to simulate the surface reflection of diffuse radiation (including multiple bouncing of light between the atmosphere and surface). How strong and important is that effect for polarization components? 4) Is 'alpha' in Eq.(1) band-dependent?

   Response:
   We have added the expression (Eq.(2)) and the detailed description for $\mathbf{R}_{\mathrm{pol}}$ in the revised manuscript.

The revised manuscript starts from next page.

Aerosol retrievals from different polarimeters during the ACEPOL campaign using a common retrieval algorithm

Guangliang Fu[1], Otto Hasekamp[1], Jeroen Rietjens[1], Martijn Smit[1], Antonio Di Noia[2], Brian Cairns[3], Andrzej Wasilewski[4], David Diner[5], Felix Seidel[5], Feng Xu[6], Kirk Knobelspiesse[7], Meng Gao[7], Arlindo da Silva[7], Sharon Burton[8], Chris Hostetler[8], John Hair[8], and Richard Ferrare[8]

[1]Netherlands Institute for Space Research (SRON, NWO-I), Utrecht, The Netherlands.
[2]University of Leicester.
[3]NASA Goddard Institute for Space Studies (GISS).
[4]Trinnovim LLC.
[5]NASA Jet Propulsion Laboratory (JPL).
[6]School of Meteorology, The University of Oklahoma National Weather Center.
[7]NASA Goddard Space Flight Center.
[8]NASA Langley Research Center.

Correspondence: Guangliang Fu (g.fu@sron.nl), Otto Hasekamp (o.hasekamp@sron.nl)

Abstract.

In this paper, we present aerosol retrieval results from the ACEPOL (Aerosol Characterization from Polarimeter and Lidar) campaign, which was a joint initiative between NASA and SRON - Netherlands Institute for Space Research. The campaign took place in October-November 2017 over the western part of the United States. During ACEPOL six different instruments were deployed on the NASA ER-2 high altitude aircraft, including four Multi-Angle Polarimeters (MAPs): SPEX airborne, the Airborne Hyper Angular Rainbow Polarimeter (AirHARP), the Airborne Multi-angle SpectroPolarimeter Imager (AirMSPI), and the Research Scanning Polarimeter (RSP). Also, two lidars participated: the High Spectral Resolution Lidar -2 (HSRL-2) and the Cloud Physics Lidar (CPL). Flights were conducted mainly for scenes with low aerosol load over land but also some cases with higher AOD were observed. We perform aerosol retrievals from SPEX airborne, RSP (410-865 nm range only), and AirMSPI using the SRON aerosol retrieval algorithm and compare the results against AERONET and HSRL-2 measurements (for SPEX airborne and RSP). All three MAPs compare well against AERONET for the Aerosol Optical Depth (AOD) (Mean Absolute Error (MAE) between 0.014-0.024 at 440 nm). For the fine mode effective radius the MAE ranges between 0.021-0.028 micron. For the comparison with HSRL-2 we focus on a day with low AOD (0.02-0.14 at 532 nm) over the California Central Valley, Arizona and Nevada (26 October) and a flight with high AOD (including measurements with AOD > 1.0 at 532 nm) over a prescribed forest fire in Arizona (9 November). For the day with low AOD the MAE in AOD (at 532 nm) with HSRL-2 are 0.014 and 0.022 for SPEX and RSP, respectively, showing the capability of MAPs to provide accurate AOD retrievals for the challenging case of low AOD over land. For the retrievals over the smoke plume also a reasonable agreement in AOD between the MAPs and HSRL-2 was found (MAE 0.088 and 0.079 for SPEX and RSP, respectively), despite the fact that the comparison is hampered by large spatial variability in AOD throughout the smoke plume. Also a good comparison is found between the MAPs and HSRL-2 for the aerosol depolarization ratio (a measure for particles sphericity) with MAE of

0.023 and 0.016 for SPEX and RSP, respectively. Finally, SPEX and RSP agree very well for the retrieved microphysical and optical properties of the smoke plume.

1 Introduction

Aerosols such as smoke, sulphate, dust, and volcanic ash particles affect the Earth climate directly by interaction with radiation and indirectly by modifying the cloud properties. In contrast to the warming effect of greenhouse gases, which is understood quite well, the quantification of aerosol cooling contains a large uncertainty, as reported in the latest (5th) assessment report of the Intergovernmental Panel on Climate Change (IPCC, 2014). This large uncertainty adds substantial difficulties in the prediction of the Earth's climate change in future. Aerosols also have a big influence on air quality. Air pollution from aerosols may result in severe adverse problems to human health (Wyzga and Rohr, 2015). To improve our understanding of the aerosol effect on climate and air quality, accurate global measurements of aerosol optical properties (e.g., aerosol optical depth (AOD), single scattering albedo (SSA)), microphysical properties (size distribution, refractive index, particles shape), and their vertical distribution, are of crucial importance. Satellite instruments are needed to obtain such measurements at a global scale.

Lidar measurements are needed to obtain vertical profile information about aerosols. The Cloud-Aerosol Lidar with Orthogonal Polarization (CALIOP) elastic backscatter Lidar (Winker et al., 2010), has been providing aerosol Lidar measurements since 2006. High Spectral Resolution Lidar (HSRL) techniques (Hair et al., 2008) are being used for the new generation of Lidar instrumentation such as the Cloud-Aerosol Transport System (CATS) instrument (Yorks et al., 2014), which has been operational on the International Space Station (ISS) in the period 2015-2017, and for the European Space Agency (ESA) Earthcare mission (Illingworth et al., 2014), expected for launch in 2021. In comparison to elastic backscatter lidars, the HSRL technique has an additional filtered channel that provides an assessment of aerosol extinction. It also improves the accuracy of the aerosol backscatter profile, especially at altitudes far from the instrument, since it is calculated as a direct ratio of two channels instead of retrieved with assumptions that result in accumulating errors. The HSRL methodology also improves the aerosol depolarization through the improved backscatter and provides the aerosol lidar ratio using the extinction (Burton et al., 2012).

From a passive remote sensing point-of-view, instruments that measure both intensity and polarization and observe a ground pixel under multiple viewing angles contain the richest set of information about aerosols in our atmosphere (Dubovik et al., 2019). The reason is that the angular dependence of the scattering matrix elements related to linear polarization, depend strongly on the microphysical aerosol properties, like refractive index and particle size (Hansen and Travis, 1974; Mishchenko and Travis, 1997). Furthermore, the polarization signal is mostly dominated by light that has been scattered only once, which means that the characteristics of the scattering matrix remain largely preserved in a top-of-atmosphere polarization measurement. The added value of polarization has been demonstrated by a number of studies on synthetic measurements (Mishchenko and Travis, 1997; Hasekamp and Landgraf, 2007; Hasekamp, 2010; Knobelspiesse et al., 2012), airborne measurements (Chowdhary et al., 2005; Waquet et al., 2009; Xu et al., 2017; Wu et al., 2015, 2016), and spaceborne measurements (Hasekamp et al., 2011b; Dubovik et al., 2011; Fu and Hasekamp, 2018). These algorithms can be divided in two main groups: LookUp-Table (LUT)

based approaches and full inversion approaches. Generally speaking, LUT approaches are faster but less accurate than full inversion approaches because LUT approaches choose the best fitting aerosol model from a discrete lookup table. Full inversion approaches are more accurate but slower because they require radiative transfer calculations as part of the retrieval procedure. The LUT algorithms are e.g., the LOA LUT algorithm over ocean (Deuzé et al., 2000), the LOA LUT algorithm over land (Deuzé et al., 2001; Herman et al., 1997), and the SSA LUT algorithm (Waquet et al., 2016). The full inversion algorithms are e.g., the GRASP algorithm (Dubovik et al., 2011), the SRON-Aerosol algorithm (Hasekamp and Landgraf, 2007; Hasekamp et al., 2011b; Stap et al., 2015; Wu et al., 2015, 2016; Di Noia et al., 2017; Fu and Hasekamp, 2018), the JPL algorithm (Xu et al., 2017), the GISS algorithm (Waquet et al., 2009) and the MAPP algorithm (Stamnes et al., 2018). Besides, some additional aerosol retrieval approaches can be found in (Sano et al., 2006; Cheng et al., 2011; Masuda et al., 2000; Lebsock et al., 2007). It should be noted that of the full inversion approaches only the SRON-Aerosol algorithm and the GRASP algorithm have been applied at a global scale.

The best known satellite instruments that performed multi-angle photopolarimetric measurements of the Earth atmosphere were the POLDER (Polarization and Directionality of the Earth's Reflectances) instruments (Deschamps et al., 1994), of which the recently decommissioned POLDER-3 on board the PARASOL micro-satellite provided data from 2005-2013. Although the original algorithms for aerosol retrieval from POLDER-3 do not make full use of the information contained in the MAP measurements (Deuzé et al., 2000, 2001), algorithms developed more recently (Dubovik et al., 2011; Hasekamp et al., 2011b; Fu and Hasekamp, 2018) do fully exploit the available information and provide insight in the capabilities and limitations of the POLDER-3 instrument. The advanced data products of these algorithms have been applied at global (Lacagnina et al., 2015, 2017) and regional (Chen et al., 2018) scale. The main limitation of the POLDER instruments is the limited accuracy with which the Degree of Linear Polarization (DoLP) can be measured. The DoLP accuracy is intrinsically limited by the filter wheel technology, which relies on sequential measurements of different polarization directions, in combination with a spatial under-sampling. On the other hand, the advantage of this technology is that it allows for a large swath with (almost) global coverage in a day. The POLDER design also forms the blueprint for the 3MI instruments (Fougnie et al., 2018), to be flown on METOP-SG in the time frame ∼2020-2035.

Focus for the development of new polarimetric instrumentation has been on improved polarimetric accuracy, more viewing angles, more wavelengths, an extended spectral range, or a combination of these aspects. For a number of these instrument concepts airborne demonstrators for possible future satellite missions have been built: 1) the Research Scanning Polarimeter (RSP) (Cairns et al., 2004) which is an airborne version of the Aerosol Polarimetry Sensor (APS) (Mishchenko et al., 2007) that was lost in a failed launch in 2011. RSP measures at many viewing angles (∼150) and 9 wavelength bands between 410-2250 nm. It has a demonstrated DoLP accuracy of better than 0.002 (Knobelspiesse et al., 2019). 2) The Airborne Multiangle SpectroPolarimetric Imager (AirMSPI) (Diner et al., 2013). AirMSPI is an eight-band (355, 380, 445, 470, 555, 660, 865, 935 nm) pushbroom camera, measuring polarization in the 470, 660, and 865 nm bands, mounted on a gimbal to acquire multiangular observations over a $\pm 67^\circ$ along-track range. The AirMSPI concept will be implemented in a satellite mission as the Multi-Angle Imager for Aerosols (MAIA) to be launched in ∼2021 (Diner et al., 2018). 3) The Airborne Hyper-Angular Rainbow Polarimeter (AirHARP) (Martins et al., 2018). AirHARP is a wide field-of-view imager that measures in

the spectral bands at 440, 550, 670, and 865 nm where 670 nm is measured under 60 and the other bands under 20 viewing geometries. This concept will be implemented in a satellite instrument for a Cubesat mission to be launched in 2019 and for the Phytoplankton Aerosol Cloud and ocean Ecosystems (PACE) mission, to be launched 2022 (Werdell et al., 2019). 4) The Spectro-polarimeter for Planetary Exploration (SPEX airborne) instrument (Smit et al., 2019). SPEX airborne employs the spectral modulation technique (Snik et al., 2009) to accurately measure the DoLP with a spectral resolution of 10-20 nm. The intensity is being measured at higher spectral resolution of 2-3 nm. SPEX airborne performs multi-angle measurements at 9 viewing angles ranging between $\pm 56^{\circ}$ in a spectral range between 400-800 nm. The SPEX concept will be implemented in a satellite instrument SPEXone (Hasekamp et al., 2019) for the NASA PACE mission (Werdell et al., 2019).

All 4 airborne MAPs listed above were mounted on the NASA Earth Resources-2 (ER-2) high altitude ($\sim$20 km) aircraft (Navarro, 2007) during the Aerosol Characterization from Polarimeter and Lidar (ACEPOL) campaign, which was performed from October-November 2017, starting from the NASA Armstrong airbase in Palmdale, California. During ACEPOL, also two lidars were deployed on the ER-2: the High Spectral Resolution Lidar-2 (HSRL-2) (Hair et al., 2008), providing vertically resolved measurements of backscatter coefficients (at 355, 532, and 1064 nm), extinction coefficients (at 355 and 532 nm), and depolarization ratio (at 355, 532, and 1064 nm) and the Cloud Physics Lidar (CPL) (McGill et al., 2002), providing vertically resolved measurements of backscatter coefficients at 355, 532, and 1064 nm and depolarization ratio at 1064 nm.

The goals of the ACEPOL campaign include: (i) comparison of level-1 (radiance and DoLP) performance between the different MAPs, (ii) comparison of aerosol retrievals from the different MAPs, (iii) comparing MAP retrievals to lidar retrievals, and (iv) performing combined retrievals using both MAP and lidar measurements. The focus of this paper is on aspects (ii) and (iii): We will perform aerosol retrievals from RSP, SPEX airborne, and AirMSPI measurements during ACEPOL, and evaluate the retrievals against AERONET and against HSRL-2. Note that aerosol retrievals from AirHARP measurements are not included in this paper, because the data were not available when performing the here presented analysis.

In this study, we evaluate the performance of the different MAPs for retrieving aerosol optical and microphysical properties, and also their capabilities to provide lidar related aerosol properties. The retrieved aerosol properties are validated and compared with the data from AERONET and HSRL-2. The paper is organized as follows. Section 2 introduces the methodologies of the SRON algorithm for polarimetric aerosol retrievals, section 3 describes the data sets from the ACEPOL campaign, which are used in this study, and the retrievals of different MAPs from ACEPOL are performed and compared with AERONET and HSRL-2 in section 4. Finally, the last section summarizes and concludes this study.

2 Methodology

2.1 SRON multimode retrieval algorithm

In this paper, we employ the SRON aerosol retrieval algorithm in multimode setup (Fu and Hasekamp, 2018). In principle, the idea of the multimode approach is that instead of fitting the size distribution parameters (the effective radius r_{eff} and the effective variance v_{eff}) of two modes, one aims to fit the size distribution with a larger number of modes for which r_{eff} and v_{eff} are fixed. The advantage of this approach is that it makes the inversion problem more linear since r_{eff} and v_{eff} tend to

make the inversion highly nonlinear. Another advantage is that the multimode approach has more freedom in fitting different shapes of size distribution if the number of chosen modes is sufficiently large. In this paper, multimode retrievals based on 5 modes are used and the aerosol size distribution are described in Table 1 (Fu and Hasekamp, 2018). We consider mode 1-3 together as the fine mode and mode 4 and 5 together as the coarse mode. To account for spectral dependence, we describe the refractive index m for the fine and coarse mode as $m(\lambda) = \sum_{k=1}^{n_\alpha} \alpha_k \, m^k(\lambda)$ where $m^k(\lambda)$ are prescribed refractive indices as function of wavelength and α_k are coefficients to be determined in the retrieval (see below). Both real part and imaginary part of refractive indices are represented in this way. Here, we base the spectral dependence of the refractive index of the standard types of D'Almeida et al. (1991) (Inorganic/Sulphate, Black Carbon, and Dust). The coefficients α_k are the real numbers between 0 and 1, and are defined as weighting factors to combine the refractive index spectra for different aerosol components, e.g., DUST, water (H2O), Black Carbon (BC), INORGanic matter (INORG). In this study, we set $n_\alpha = 2$ and assume that spectral dependence of the fine mode and the coarse mode refractive indices can be described respectively by INORG+BC and DUST+INORG. Note that this assumption is flexible and can be updated according to the information content of the measurement. Also spectra based on Principal Component Analysis (PCA) can be used as in Wu et al. (2015). The standard refractive index spectra are only used to describe the spectral dependence as the MAP measurements do not contain sufficient information to retrieve the refractive index for each wavelength separately. Nonspherical aerosols are described as a size/shape mixture of randomly oriented spheroids (Hill et al., 1984; Mishchenko et al., 1997). We use the Mie/T-matrix-improved geometrical optics database by Dubovik et al. (2006) along with their proposed spheroid aspect ratio distribution for computing optical properties for a mixture of spheroids and spheres. The aerosol parameters included in the retrieval state vector $\boldsymbol{x}$ are the aerosol column numbers for the 5 modes (Table 1), 2 coefficients (Inorganic, Black Carbon) for the fine mode refractive index, 2 coefficients (Inorganic, Dust) for the coarse mode refractive index, the fraction of spherical particles (assumed the same for all modes), and the central height of a Gaussian aerosol height distribution (assumed the same for all modes).

For the surface reflection matrix we use (Rahman et al., 1993; Litvinov et al., 2011; Xu et al., 2017):

$$\mathbf{R}_s(\lambda, \mu_{\rm in}, \mu_{\rm out}, \phi_v - \phi_0) = A(\lambda) \left(\frac{(\mu_{\rm in}\, \mu_{\rm out})^{k-1}}{(\mu_{\rm in} + \mu_{\rm out})^{1-k}} \, F(g, \Theta)[1 + R(G)] \right) \mathbf{D} + \mathbf{R}_{\rm pol} \tag{1}$$

$$\mathbf{R}_{\rm pol}(\mu_{\rm in}, \mu_{\rm out}, \phi_v - \phi_0) = B \left(\frac{\exp\left(-\tan(\frac{\pi - \Theta}{2})\right) \, \exp(-\nu) \, F_p(m, \Theta)}{4(\mu_{\rm in} + \mu_{\rm out})} \right) \tag{2}$$

where k is a parameter that varies between 0 and 1. This parameter controls the slope of the reflectance with respect to the illumination and view angles (Rahman et al., 1993). $\mathbf{D}$ is the null matrix except $\mathbf{D}_{11}$ = 1. The first part in Eq. (1) accounts for the bidirectional reflectance distribution function (BRDF) parameterized by the Rahman-Pinty-Verstraete (RPV) model (Rahman et al., 1993). The pairs (θ_0, ϕ_0) and (θ_v, ϕ_v) respectively denote the solar and viewing zenith and azimuth angles. $\mu_{\rm in}$ and $\mu_{\rm out}$ are respectively the cosines of incoming and outgoing angles. g is the asymmetry parameter of the Henyey-Greenstein phase function $F(g, \Theta)$. Θ is the scattering angle. $1 + R(G)$ is an approximation of the hot spot effect (Rahman et al., 1993), where $G = \sqrt{\tan^2\theta_0 + \tan^2\theta_v - 2\tan\theta_0 \tan|\theta_v| \cos(\phi_v - \phi_0)}$ and $R(G) = \frac{1 - A(\lambda)}{1 + G}$. The second part in Eq. (1) accounts for

the surface polarized reflectance, where we use the model proposed by Maignan et al. (2009). $\mathbf{R}_{\rm pol}$ is expressed by Eq. (2) (as stated by Eq. (31) in Litvinov et al. (2011)). Here, B is a scaling parameter (band-independent). $F_p(m,\Theta)$ is the element F_{21} of the Fresnel scattering matrix with refactive index m. Parameter ν is taken based on Atmospherically Resistant Vegetation Index (ARVI) (Kaufman and Tanre, 1992). Here we use $\nu = 0.6$. Based on Eq. (1) and Eq. (2), We include $A(\lambda)$ at each measured wavelength, and k, g, and B as fit parameters in the state vector. In this paper, we perform aerosol retrievals from SPEX airborne, RSP, and AirMSPI, and the state vectors corresponding to these three polarimeters are listed in Table 2.

The measurement vector $\boldsymbol{y}$ contains the measured radiances (sun normalized) and Degree of Linear Polarization (DoLP) values at the different wavelengths and viewing angles. To retrieve the state vector from the measurements, a damped Gauss-Newton iteration method with Phillips-Tikhonov regularization is employed (Hasekamp et al., 2011b; Fu and Hasekamp, 2018). The inversion algorithm finds the solution $\hat{\boldsymbol{x}}$, which solves the minimization-optimization problem,

$$\hat{\boldsymbol{x}} = \min_{\boldsymbol{x}}(||\mathbf{S}_y^{-\frac{1}{2}}(\mathbf{F}(\boldsymbol{x}) - \boldsymbol{y})||^2 + \gamma^2||\mathbf{W}^{-\frac{1}{2}}(\boldsymbol{x} - \boldsymbol{x}_{\rm a})||^2). \tag{3}$$

Here, $\mathbf{F}$ is the forward model that simulates the measurement for a given state vector $\boldsymbol{x}$. $\mathbf{F}$ consists of a radiative transfer model, for which we use the SRON radiative transfer model LINTRAN Landgraf et al. (2001); Hasekamp and Landgraf (2002, 2005); Schepers et al. (2014). All the radiative transfer calculations are performed for a model atmosphere that includes Rayleigh scattering, scattering and absorption by aerosols, and gas absorption. Rayleigh scterring cross sections are used from Bucholtz (1995). The forward model simulates Stokes parameters I, Q, U at the height of the observation (e.g., $\sim$20 km for NASA ER-2 in this paper) for given optical properties (scattering and absorption optical thickness and scattering phase matrix for each vertical layer of the model atmosphere (- 15 layers of atmosphere is assumed). The other part of the forward model computes the optical properties from the aerosol microphysical properties using the tabulated kernels of Dubovik et al. (2006) for a mixture of spheroids and spheres.

Since the forward model is nonlinear the inversion problem has to be solved iteratively replacing the forward model in each iteration step by its linear approximation,

$$\mathbf{F}(\boldsymbol{x}) \approx \mathbf{F}(\boldsymbol{x}_n) + \mathbf{K}(\boldsymbol{x} - \boldsymbol{x}_n). \tag{4}$$

Here, $\mathbf{K}$ is the Jacobian matrix (with $K_{ij} = \frac{\partial F_i}{\partial x_j}(\boldsymbol{x}_n)$), which contains the derivatives of the forward model with respect to each variable in the state vector $\boldsymbol{x}$. Therefore, the optimization problem (Eq. (3)) is reduced to

$$\tilde{\boldsymbol{x}}_{n+1} = \min_{\tilde{\boldsymbol{x}}}(||\tilde{\mathbf{K}}(\tilde{\boldsymbol{x}} - \tilde{\boldsymbol{x}}_n) - \tilde{\boldsymbol{y}}||^2 + \gamma^2||\tilde{\boldsymbol{x}} - \tilde{\boldsymbol{x}}_a||^2), \tag{5}$$

where $\tilde{\mathbf{K}} = \mathbf{S}_y^{-\frac{1}{2}}\mathbf{K}\mathbf{W}^{\frac{1}{2}}$, $\tilde{\boldsymbol{x}} = \mathbf{W}^{-\frac{1}{2}}\boldsymbol{x}$ and $\tilde{\boldsymbol{y}} = \mathbf{S}_y^{-\frac{1}{2}}(\boldsymbol{y} - \mathbf{F}(\boldsymbol{x}_n))$. $\boldsymbol{x}_{\rm a}$ is the a priori state vector, $\mathbf{W}$ is a weighting matrix that ensures that all state vector parameters range within the same order of magnitude (Hasekamp et al., 2011b), and $\mathbf{S}_y$ is the measurement error covariance matrix. Table 2 shows the values of $\boldsymbol{x}_{\rm a}$ for aerosol and surface parameters. $\mathbf{W}$ is a diagonal matrix and its diagonal values are also shown in Table 2 (in the "weight" column). The solution of Eq. (5) is given by:

$$\tilde{\boldsymbol{x}}_{n+1} = \tilde{\boldsymbol{x}}_n + \Lambda(\tilde{\mathbf{K}}^T\tilde{\mathbf{K}} + \gamma^2\mathbf{I})^{-1}(\tilde{\mathbf{K}}^T\tilde{\boldsymbol{y}} - \gamma^2(\tilde{\boldsymbol{x}}_n - \tilde{\boldsymbol{x}}_a)). \tag{6}$$

Λ is a filter/damping factor, which limits the step size for each iteration of the state vector. In this way, we use a Gauss-Newton scheme with reduced step size to avoid diverging retrievals (Hasekamp et al., 2011a). The filter factor Λ values between 0 and 1. The regularization parameter γ^2 in Eq. (3) is chosen optimally (for each iteration) from different values (5 values from 0.1 to 5) by evaluating the goodness of fit using a simplified (fast) forward model. In the SRON aerosol algorithm, the first guess is obtained before the full inversion retrieval using a multimode Look-Up Table (LUT), which is based on tabulated RT calculations for each mode. The pre-calculated LUT is used as input for an approximate forward model in the LUT retrieval. Here, single scattering is computed exactly as its computational cost is negligible. The fit parameters in the LUT retrieval are the aerosol column numbers for each mode and the surface parameters. For the first guess of the refractive index we use a fixed value of 1.45 for all modes. For further details we refer to Fu and Hasekamp (2018).

We use the goodness of fit (χ^2) to decide whether the retrievals have successfully converged:

$$\chi^2 = \frac{1}{n_{\text{meas}}} \sum_{i=1}^{n_{\text{meas}}} \frac{(F_i - y_i)^2}{S_y(i,i)}. \tag{7}$$

Here, n_{meas} is the total number of measurements (multi-angle and multispectral radiance and DoLP) for each pixel. We consider valid retrievals those that achieve a χ^2 smaller than an empirically chosen threshold χ^2_{max}. This filter rejects cases in which the forward model is not able to fit the measurements, e.g., because of cloud-contaminated pixels (Stap et al., 2015, 2016), corrupted measurements (Hasekamp et al., 2011b), and cases in which the first guess state vector deviates too much from the truth (Di Noia et al., 2015).

2.2 Fine mode and coarse mode effective radius

According to Eq. (2.53) in (Hansen and Travis, 1974), the effective radius is defined:

$$r_{\text{eff}} = \frac{\int_{r_{\min}}^{r_{\max}} \pi r^3 n(r) dr}{\int_{r_{\min}}^{r_{\max}} \pi r^2 n(r) dr} = \frac{R}{O} \tag{8}$$

where $n(r)dr$ is the number of particles with radius between r and $r+dr$. $r_{\min}$ and $r_{\max}$ are the particle radius for the smallest and largest particles.

In this study, a 5-mode retrieval is used. The effective radius for multiple modes together ($r^{\text{m}}_{\text{eff}}$) is calculated from the different fixed modes by: $r^{\text{m}}_{\text{eff}} = \frac{\sum_{n^{\text{m}}} R_i}{\sum_{n^{\text{m}}} O_i}$ where n^{m} is the number of modes grouped together. For the 5-mode retrievals in this study, we compute r_{eff} for the fine mode (modes 1-3 together) and and coarse mode (modes 4 and 5 together).

2.3 Aerosol depolarization ratio and aerosol lidar ratio

The aerosol lidar properties are related to the aerosol scattering matrix. For some general assumptions ((i) scattering by an assembly of randomly oriented particles each having a plane of symmetry, (ii) scattering by an assembly containing particles and their mirror particles in equal numbers and with random orientations, (iii) Rayleigh scattering with or without depolarization effects), the aerosol scattering matrix has a simplified block-diagnonal structure (Bottiger et al., 1980; Mishchenko, 2014):

$$\mathbf{F}(\Theta) = \begin{bmatrix} F_{11}(\Theta) & F_{12}(\Theta) & 0 & 0 \\ F_{12}(\Theta) & F_{22}(\Theta) & 0 & 0 \\ 0 & 0 & F_{33}(\Theta) & F_{34}(\Theta) \\ 0 & 0 & -F_{34}(\Theta) & F_{44}(\Theta) \end{bmatrix} \tag{9}$$

where Θ is the scattering angle and F_{11} is the phase function for total radiance.

The aerosol (linear) depolarization ratio is defined as:

$$\delta_{\mathrm{col}}^{\mathrm{pol}} = \frac{F_{11}(180^\circ) - F_{22}(180^\circ)}{F_{11}(180^\circ) + F_{22}(180^\circ)} \tag{10}$$

which is adpated from Eq. (3) in (Mishchenko et al., 2016). We use Eq. (10) to compute an aerosol depolarization ratio from the aerosol properties of the MAPs and compare this to the vertically integrated value measured by HSRL-2, which is calculated by:

$$\hat{\delta}^{\mathrm{hsrl}}(i) = \frac{\delta^{\mathrm{hsrl}}(i)}{1+\delta^{\mathrm{hsrl}}(i)}, \qquad \hat{\delta}_{\mathrm{col}}^{\mathrm{hsrl}} = \frac{\sum_{i=0}^{n_{\mathrm{bin}}} (\hat{\delta}^{\mathrm{hsrl}}(i)\ \beta_{\mathrm{b}}^{\mathrm{hsrl}}(i))}{\sum_{i=0}^{n_{\mathrm{bin}}} (\beta_{\mathrm{b}}^{\mathrm{hsrl}}(i))}, \qquad \delta_{\mathrm{col}}^{\mathrm{hsrl}} = \frac{\hat{\delta}_{\mathrm{col}}^{\mathrm{hsrl}}}{1-\hat{\delta}_{\mathrm{col}}^{\mathrm{hsrl}}}, \tag{11}$$

where $i = 0$ corresponds to the bin closet to the surface, $i = n_{\mathrm{bin}}$ corresponds to the bin closet to the aircraft. The aerosol backscatter coefficient ($\beta_{\mathrm{b}}^{\mathrm{hsrl}}(i)$) for each bin is used as the weighting parameter. $\delta^{\mathrm{hsrl}}(i)$ is first transformed to $\hat{\delta}^{\mathrm{hsrl}}(i)$, which is because $\hat{\delta}^{\mathrm{hsrl}}(i)$ mix linearly like backscatter, but $\delta^{\mathrm{hsrl}}(i)$ does not (Burton et al., 2014).

In our retrieval algorithm we assume that for aerosols the single scattering albedo ω and F_{11} do not depend on altitude. In that case, using ω and $F_{11}(180^\circ)$, we compute the vertically integrated aerosol extinction-to-backscatter ratio, i.e., aerosol lidar ratio for a MAP by:

$$S_{\mathrm{col}}^{\mathrm{pol}} = \frac{4\pi}{\omega\ F_{11}(180^\circ)}, \tag{12}$$

which is adpated from Eq. (4) in Lopes et al. (2013). This can be compared to the corresponding value from HSRL-2:

$$S_{\mathrm{col}}^{\mathrm{hsrl}} = \frac{\sum_{i=0}^{n_{\mathrm{bin}}} (\beta_{\mathrm{e}}^{\mathrm{hsrl}}(i))}{\sum_{i=0}^{n_{\mathrm{bin}}} (\beta_{\mathrm{b}}^{\mathrm{hsrl}}(i))} \tag{13}$$

which is adapted from Eq. (28) in Stamnes et al. (2018). Here $\beta_{\mathrm{e}}^{\mathrm{hsrl}}(i)$ denotes the extinction coefficient for each bin.

3 Measurements

For this study, we use airborne measurements from 3 different polarimeters (SPEX airborne, RSP, AirMSPI) and one lidar (HSRL-2). Further, we use ground based measurements for validation and re-analysis data as input to our retrieval algorithm. All data are described in this section.

3.1 RSP

RSP (Cairns et al., 1999) started to operate on the NASA ER-2 since 2010 and has flown on a number of other airplanes since 2001 (Cairns et al., 2003). Multi-viewing capability over a large along-track angular range and at many viewing angles (~ 150) is obtained using a scanning mirror. Due to the fact that some viewing angles are blocked by the aircraft, the angular range of RSP on the ER-2 is restricted to -40° to 60°. The Stokes parameters Q and U are analyzed in separate refractive telescopes, using Wollaston prisms, followed by dichroic beamsplitters. The RSP instrument is equipped with an in-flight calibration system, and the accuracy for the DoLP is better than 0.002 (Knobelspiesse et al., 2019), providing a benchmark (in DoLP) for other MAPs. Aerosol retrievals from RSP have been performed, amongst others, by Waquet et al. (2009); Wu et al. (2015, 2016); Di Noia et al. (2017); Stamnes et al. (2018); Gao et al. (2019).

A complicating factor for using RSP measurements in aerosol retrievals over inhomogeneous land surfaces is that different viewing angles have different ground pixel size and may look at slightly shifted scenes on the ground. To partly overcome this problem we use (1) the approach of Wu et al. (2015) and construct RSP pixels that represent a 5 km along track running average; (2) the (moving average) approach of Di Noia et al. (2017) to select 10 viewing angles covering a broad viewing angle range (over the total RSP viewing angles) and convolve RSP measurements at each selected angle with an average of 5 angles. In this sense, although averaged measurements 10 viewing angles are input to the retrieval algorithm, they are constructed from original RSP measurements at 50 angles. In this study, we use 5 wavelengths (410, 469.1, 554.9, 670, and 863.4 nm) for RSP retrievals as Di Noia et al. (2017). The viewing angles and wavelengths used in retrievals are summarized in Table 2. It should be noted that theoretically the SWIR bands of RSP 1590 and 2250 nm would provide extra constraints for the characterization of coarse mode aerosols. For the ACEPOL campaign however, we found no improvement by including the SWIR bands, and even slightly worse results (compared to AERONET and HSRL-2) in some cases. A possible explanation is that our assumption that the directional property of surface reflection is spectrally neutral does not hold over the full RSP wavelength range. Another explanation may be that the SWIR channels are affected by gas absorption which we could not perfectly correct for.

3.2 AirMSPI

AirMSPI (Diner et al., 2013) started to operate on the NASA ER-2 since October 2010. AirMSPI is an eight-band (355, 380, 445, 470, 555, 660, 865, 935 nm) pushbroom camera, which measures linear polarization in the 470, 660, and 865 nm bands. AirMSPI employs a photoelastic modulator-based polarimetric imaging technique to enable accurate measurements of Degree of Linear Polarization (DoLP) in addition to intensity. The instrument is mounted on a gimbal to acquire multiangular observations in the range of $\pm 67°$. AirMSPI has two principal observing modes: (1) step-and-stare, where 11 km$\times$ 11 km targets are observed at a discrete set of view angles with a spatial resolution of ~ 10 m. (2) continuous sweep, where the camera slews back and forth along the flight track between $\pm 65°$ to acquire wide area coverage (11 km swath at nadir, target length 108 km). The spatial resolution is ~ 25 m. Aerosol retrievals from AirMSPI have been performed by Xu et al. (2017, 2018, 2019). In this study, only the step-and-stare measurements have been used as they provide a mult-angle-view of the same ground scene. For ACEPOL, AirMSPI was programmed to measure at 9 viewing angles in the step-and-stare mode: 0° (nadir),

$\pm 29°$, $\pm 48°$, $\pm 59°$, $\pm 66°$. Radiance measurements are used at all wavelengths except 935 nm and DoLP measurements at all 3 wavelengths. The viewing angles and wavelengths used in retrievals are summarized in Table 2. Following Xu et al. (2017), for AirMSPI we aggregate individual ground pixels to 1 km$\times$ 1 km spatial grid in order to be less affected by surface inhomogeneity and its effect on the angular co-registration.

3.3 SPEX airborne

SPEX airborne performed its first (engineering) flight on the ER-2 in 2016. ACEPOL has been the first full science campaign. The instrument employs the spectral modulation technique (Snik et al., 2009) to accurately measure the Degree of Linear Polarization (DoLP) in the spectral range 400-800 nm with a spectral resolution of 10-20 nm, and the intensity at a higher spectral resolution of 2-3 nm. A ground-based version of SPEX has performed upward looking measurements from the ground which have been used to successfully retrieve aerosol microphysical and optical properties by van Harten et al. (2014); Di Noia et al. (2015). SPEX airborne performs multi-angle measurements at 9 viewing angles: $\pm 56°$, $\pm 42°$, $\pm 28°$, $\pm 14°$, and $0°$. Smit et al. (2019) performed a comparison between SPEX airborne and RSP for radiance and DoLP measurements at 410, 470, 550, and 670 nm. They found very good agreement between SPEX airborne and RSP at 550 and 670 nm whereas the agreement gets worse towards smaller wavelengths. In this study, we use measurements of radiance and DoLP at 16 wavelengths, (450, 460, 470, 480, 490, 500, 510, 520, 530, 540, 550, 565, 580, 600, 670, and 750 nm). The measurement at each wavelength represents an average of a 10 nm wide spectral region. We leave out the shortest wavelengths because of less good agreement with RSP, and the wavelengths $>$750 nm because of order overlap of the grating. The viewing angles and wavelengths used in retrievals are summarized in Table 2.

Each SPEX viewport has a moderate swath of $\sim$ 6 degrees (Smit et al., 2019) in the across-track direction, which translates to a projected field of view from 2.4 km at nadir to 4.5 km at fore and aft viewports when the instrument is operated at the typical altitude of ER-2. Conceptually, the instrument acts as nine separate pushbroom spectrometers, which produce nine overlapping strips of data on the ground. In this way, a multi-angular view is obtained of ground scenes when the aircraft flies over it. The spatial sampling of the L1C product is chosen as 1 km$\times$ 1 km (across $\times$ along-track), which is driven by the L1B spatial resolution of the outer viewports.

3.4 HSRL-2 data

The NASA Langley HSRL-2 instrument, operational since 2012, is a successor to the NASA Langley airborne HSRL-1 instrument, which was described by Hair et al. (2008); Burton et al. (2012) and validated by Rogers et al. (2009). The HSRL-2 uses the HSRL technique to independently measure aerosol extinction and backscatter at 355 nm (Burton et al., 2018) and 532 nm and the standard backscatter technique to measure aerosol backscatter at 1064 nm (Müller et al., 2014). It is polarization sensitive at all three wavelengths. HSRL-2 measures vertically resolved values for the backscatter coefficient (β) and aerosol depolarization ratio at 355, 532, and 1064 nm (Burton et al., 2015) and the extinction coefficient and AOD at the high-spectral-resolution channels, 355 and 532 nm. HSRL-2 is the first airborne system capable of providing 3 backscatter and 2 extinction measurements, which is important for lidar retrievals of microphysical properties (Müller et al., 2014).

For the ACEPOL flights on the ER-2, the aerosol backscatter coefficient is derived using the HSRL technique at 355 nm and 532 nm and the elastic backscatter technique at 1064 nm and reported at a vertical resolution of 15 m and a horizontal/temporal resolution of 10 seconds (approximately 1-2 km at ER-2 cruise speeds). The aerosol depolarization ratios at all 3 wavelengths are reported at the same resolutions. For ACEPOL, the extinction products from the HSRL method are reported at 150 m vertical resolution and at temporal resolution of 60 s generally and 10 s. Additionally, the aerosol extinction products at 355 nm and 532 nm are also provided based on the aerosol backscatter and an assumed lidar ratio of 40 sr, and reported at the backscatter resolution.

Similarly, the AOD is reported from the standard HSRL approach and also the AOD calculated using the assumed lidar ratio is provided. The reason why two AOD products are reported is that during ACEPOL, HSRL-2 experienced an interference that appears to be related to atmospheric turbulence. This interference impacted the ability to use the 532 nm and 355 nm molecular channels to derive aerosol extinction and AOD from the usual HSRL method. However, this interference did not impact the measurements of aerosol backscatter profiles and so these profiles were computed using the HSRL technique (i.e. ratio of total backscatter to molecular backscatter). The systematic uncertainties on the AOD from the HSRL method is about 0.05 for ACEPOL, whereas the assumed lidar ratio produces systematic uncertainty that is a constant relative fraction ($\pm$ 50%). Therefore, for the case with high AOD (i.e., Figs 7 and 8), the uncertainty is smaller when using the HSRL method and we therefore use these products for this case. Conversely, although the uncertainties are fairly high for both products for low AOD, the product using an assumed lidar ratio is expected to have lower uncertainties, and we use these products for the low AOD cases (i.e., Figs 4, 5, and 6) in this paper.

3.5 AERONET data

The multispectral aerosol optical depth (AOD) from the MAP and lidar retrievals is validated with AERONET (AErosol RObotic NETwork) level 1.5 data (Holben et al., 2001) (version 3.0). The data are cloud cleared. The uncertainty on AERONET AOD is 0.01 for mid-visible wavelengths and 0.03 for UV wavelengths (Eck et al., 1999) and is dominated by a calibration (systematic) error. The effective radius for fine and coarse modes are compared with AERONET level 1.5 Almucantar Retrieval Inversion Products (Dubovik et al., 2002). The AOD of fine and coarse modes are compared with AERONET level 1.5 spectral de-convolution algorithm (SDA) data (O'Neill et al., 2003). It should be noted that the inversion- and SDA products are quite uncertain themselves at low AOD so the comparison to these products should not be considered a validation. In this paper, data from the 6 following AERONET stations are used for validation: Bakersfield, CalTech, Flagstaff ("USGS_Flagstaff_ROLO"), Fresno_2, Modesto, and Railroad-Valley.

3.6 Re-analysis data

The required meteorological inputs for our retrieval scheme are vertical profiles of humidity, temperature, and pressure. We obtain these information from National Centers for Environmental Prediction (NCEP) reanalysis data (Kalnay et al., 1996). For ozone absorption in retrievals, we use the ozone profiles from Modern-Era Retrospective analysis for Research and Ap-

plications, Version 2 (MERRA-2) (Gelaro et al., 2017). The NO_2 columns are taken from Air Force Geophysics Laboratory (AFGL) database. The data are interpolated to the specific time and location of a MAP ground pixel.

4 Results

We apply the SRON algorithm as described in section 2.1 to measurements of SPEX, RSP, and AirMSPI. In our retrievals we use an ad-hoc representation of the measurement error covariance matrix $\mathbf{S}_y$, where we assume a diagonal matrix for $\mathbf{S}_y$ (i.e. errors are uncorrelated for different wavelengths and viewing angles) with values on the diagonal corresponding to 5 % error on the radiance and 0.005 on DoLP. Although this is a crude assumption that does not reflect a bottom-up estimate taking into account individual error sources, it should be noted that for the chosen inversion approach the most important aspect is the relative dependence between radiance and DoLP errors, because we include a flexible regularization parameter that is determined as part of the retrieval. The same results can be obtained when assuming 2.5 % radiance and 0.0025 DoLP errors, in combination with a different χ^2 filter. This relative dependence between radiance and DoLP accuracies seems reasonable for all three instruments given that they all have a high DoLP accuracy. Another note is that there are error sources such as mis-registration between different viewing angles, that are not included in an uncertainty model (as they are not directly related to pure instrument performance) but that are significant and possibly even dominant over land.

To compare MAP retrievals with AERONET or HSRL-2, $\chi^2 < 1.5$ is used in this paper (for SPEX, RSP, and AirMSPI) as the filter for the goodness of fit. Besides, we also apply filters on the number of viewing angles (≥ 9), the smallest scattering angle ($< 120°$), and the largest scattering angle ($> 120°$). To evaluate the retrieved aerosol properties, three measures are used, which are the Mean Absolute Error (MAE), the Mean Relative Error (MRE), the bias, and the STandard Deviation (STD). Two types of plots are included in this paper for comparisons. One is the scatter plot with x- and y-axis respectively for two instruments. The other one is the Bland-Altman (Martin Bland and Altman, 1986) plot (difference plot), where the differences between two instruments are plotted against the the averages of the two intruments.

4.1 SPEX airborne, RSP, and AirMSPI versus AERONET

We first compare the polarimetric (SPEX, RSP, and AirMSPI) retrievals with the AERONET data for the aerosol optical depth (AOD) at three wavelengths 380 nm, 440 nm, and 675 nm. For the comparison, retrievals within 10 km around each AERONET station are selected and averaged. The AERONET data are averaged within 1 hour around the time of the ER-2 overpass. The results of the AOD comparison are shown in Figure 1 where panels a,d correspond to SPEX airborne, panels b,e to RSP, and panels c,f to AirMSPI. The 12 overpasses between SPEX and AERONET are consistent with those between RSP and AERONET, i.e., one averaged value from SPEX (Fig 1a) and RSP (Fig 1b) correspond to the same averaged value from AERONET. For AirMSPI (Fig 1c), 8 overpasses are consistent with SPEX and RSP, while the other 4 comparison points do not have corresponding points for SPEX and RSP. The reason for this inconsistency in comparison points is that AirMSPI was not making measurements for some of the AERONET overpasses. On the other hand some of the SPEX and RSP overpasses

are screened out because there were no ground pixels with enough co-located viewing angles because of aircraft yaw, while the swath of AirMSPI is sufficiently large to still get co-located angles despite the yaw.

For the AOD at 440 nm, the MAE is respectively 0.016, 0.024, 0.014, the MRE is respectively 0.175, 0.289, 0.139, the bias is respectively 0.003, -0.010, -0.004, and the STD is respectively 0.019, 0.027, 0.017 for SPEX, RSP, and AirMSPI. The MAE, bias, and STD are within 0.01 and the MRE is within 0.15 for the instruments, where the values for SPEX airborne and AirMSPI are somewhat smaller than for RSP. Similar conclusions hold for the AOD at 380 nm or 675 nm. For each instrument, the MAE gets smaller with increasing wavelengths, which is mainly caused by the fact that the AOD value itself decreases with wavelength. Based on the comparisons above, we can conclude that the SPEX, RSP, and AirMSPI all achieve good agreement with AERONET and the differences in performance between the instruments are small.

For the comparison of the fine and coarse mode effective radius ($r^{\mathrm{f}}_{\mathrm{eff}}$ and $r^{\mathrm{c}}_{\mathrm{eff}}$), it should be noted that it is difficult to retrieve them when AOD is small. Therefore, shown in Figure 2 are the comparison when τ_{380} is larger than 0.1. The remaining cases are still very challenging but we would lose too many points if we further increase the AOD limit. The solid lines shown in the plot are bias$\pm$STD. The retrievals of $r^{\mathrm{f}}_{\mathrm{eff}}$ compared with AERONET are shown in Figs. 2a-c, where the MAE is 0.022, 0.021, and 0.028 μm for SPEX, RSP, and AirMSPI, respectively. SPEX and RSP compare somewhat better in terms of MAE and bias whereas AirMSPI has a small STD. However, overall the differences between the instruments are small and the number of comparison points is very limited, which means that differences between instruments can be explained by 1 or 2 points. The $r^{\mathrm{c}}_{\mathrm{eff}}$ comparisons corresponding to SPEX, RSP, and AirMSPI are shown in Figs 2d-f, respectively. All three instruments have a poor comparison with AERONET for $r^{\mathrm{c}}_{\mathrm{eff}}$, with a MAE close to 1.5 μm. This is in line with synthetic studies (e.g., Hasekamp et al. (2019)) that $r^{\mathrm{c}}_{\mathrm{eff}}$ is a difficult parameter to retrieve, in particular for small AOD values. It should be noted that AERONET consistently gives larger coarse mode effective radius than MAPs. A possible explanation is that the effective radius for the coarse mode 4 and 5 in our 5-mode retrieval are 0.882 and 1.719 respectively (see Table 1), thus the coarse mode effective radius from MAPs calculated based on Eq. (8) is estimated and limited between 0.882 and 1.719, wheras AERONET gives values between 2.25 and 3.3 (when τ_{380} is larger than 0.1). A comparable range is expected for MAPs if a parametric 2-mode retrieval or a $\geq$7-mode retrieval (Fu and Hasekamp, 2018) is used. Also, it should be noted that the "fine" and "coarse" as defined by the Almucantar retrievals are different with defining "fine" and "coarse" by specific modes as shown in Table 1. This may introduce differences in the comparisons.

For the comparison of the fine and coarse mode AOD (τ^{f} and τ^{c}), the results are shown in Figure 3. The comparison shows a MAE of 0.028, 0.029, and 0.012 for SPEX, RSP, and airMSPI, respectively for τ^{f} and 0.026, 0.028, 0.017 for τ^{c}. The bias is 0.028, 0.019 and 0.004 for τ^{f} and 0.025, 0.028, and 0.003 for τ^{c}. So, SPEX and RSP have an overestimation of the fine mode and an underestimation of the coarse mode, compared to AERONET SDA product. Although these biases are large in a relative sense (given the low AOD, especially for the coarse mode), they are within the expected error from the AERONET SDA product. AirMSPI compares better to the AERONET SDA product than SPEX airborne and RSP. Again, it should be noted that the AirMSPI comparison does not contain exactly the same points as the comparison for SPEX and RSP. It should also be noted that for RSP, since no SWIR channels are included in the retrieval to nail the coarse mode, we thus don't expect it to do well retrieving coarse mode properties. It is important to note that for the low AOD values encountered during ACEPOL, the

AERONET retrieved fine and coarse mode AOD and effective radius are very uncertain themselves. Therefore, this comparison should not be interpreted as "retrieval versus truth" but rather as "retrieval versus retrieval".

4.2 Comparison between SPEX airborne, RSP, and HSRL-2

For the comparison to HSRL-2, we only use SPEX airborne and RSP because these provided a continuous data stream during ACEPOL, while AirMSPI only provides step-and-stare measurements for specific targets.

4.2.1 Comparison HSRL-2 to AERONET

Given that we use HSRL-2 as a reference for our MAP retrievals, it is important to first validate HSRL-2 with AERONET. Figure 4 shows the comparison of the HSRL-2 AOD at 355 nm and 532 nm with AERONET (log-log interpolated between 340 and 380 nm for 355 nm and between 500 and 675 nm for 532 nm). From the comparison it follows that the HSRL-2 AOD at 532 nm agrees very well with AERONET, with a small MAE (0.012), a small MRE (0.269) a small absolute bias (0.005), and a small STD (0.014). The comparison at 355 nm is somewhat worse than that at 532 nm with an MAE of 0.028, an MRE of 0.357, a bias of -0.014, and a STD of 0.029. The bias between HSRL-2 and AERONET is within the AERONET uncertainty. The random differences, with standard deviation 0.029 at 380 nm and 0.014 at 532 nm are most likely due to HSRL-2 uncertainties. Note that shown in Figure 4 are the points corresponding to days 23 October, 25 October, 26 October, and 7 November 2017.

4.2.2 Low AOD case on 26 October 2017

In this subsection, we compare the aerosol properties from SPEX and RSP with those from HSRL-2 for the day 26 October 2017 with low aerosol loading (AOD at 532 nm in the range 0.02 to 0.14). The results for AOD at 355 nm and 532 nm are shown in Figure 5. Figure 5a shows the retrieved AOD from HSRL-2 for the ground pixels co-located with SPEX and RSP. From this figure it follows that there were very low AOD values for the eastern part of the scene and somewhat higher values in the western and south-western part of the scene. Figure 5b shows the AOD comparison between SPEX and HSRL-2 with the MAE 0.014, the MRE 0.296, the bias 0.009, and the STD 0.018 at 532 nm, and the MAE 0.028, the MRE 0.321, the bias -0.006, and the STD 0.034 at 355 nm. Figure 5c shows the AOD comparison between RSP and HSRL-2 with the MAE 0.022, the MRE 0.418, the bias -0.007, and the STD 0.028 at 532 nm, and the MAE 0.037, the MRE 0.369, the bias -0.008, and the STD 0.048 at 355 nm. So, SPEX shows a very good agreement with HSRL-2 for this challenging scene of low AOD over land with a relatively bright surface. SPEX compares somewhat better to HSRL-2 than RSP for this case at both 532 and 355 nm. The Bland-Altman plots Figs 5e and f show a larger scatter and more outliers for RSP. A possible explanation is that for low AOD the radiance and polarization measurements have strong influence from the spatially inhomogeneous surface, and therefore errors due to inter-angle mis-registration, which are larger for RSP than for SPEX, may be significant. For these cases there is larger sensitivity to spatial mismatch between different viewing angles, and RSP, as a single-pixel-swath instrument, is more sensitive to such mismatches. Figure 5d shows the AOD comparison between SPEX and RSP with the MAE 0.024, the MRE 0.831, the bias 0.016, and the STD 0.025. The differences from the direct comparison between SPEX and RSP are somewhat

larger than those from individual comparisons with HSRL-2 of SPEX and RSP, respectively. This suggests that the differences with HSRL-2 are not caused by common assumptions in the SPEX and RSP retrievals, but are rather caused by errors that are specific to each MAP.

For the retrieved surface parameters, we do not have a good reference to evaluate the accuracy. Instead, Figure 6 shows the AOD difference between MAP and HSRL-2 as function of retrieved BRDF scaling parameter A, where we do not see clear correlation or dependence.

4.2.3 High AOD on 9 November 2017

In this subsection, polarimetric retrievals from SPEX airborne and RSP are compared to HSRL-2 on the day 9 November 2017 for a smoke plume with high AOD (including AOD values > 1.0). Figure 7a shows the original AOD (i.e., no filter or colocation included) from SPEX for the flight leg over the smoke plume. This gives a sense of how variable the smoke plume is. Figure 7b shows the AOD comparison between SPEX and HSRL-2, where the MAE is 0.088, the MRE is 0.693, the bias is -0.029, and the STD is 0.149 at 532 nm. Figure 7c shows the AOD comparison between RSP and HSRL-2, where the MAE is 0.079, the MRE is 0.564, the bias is -0.024, and the STD is 0.142 at 532 nm. Figure 7d shows the AOD comparison between SPEX and RSP, where the MAE is 0.044, the MRE is 0.155, the bias is -0.005, and the STD is 0.063 at 532 nm. RSP compares slightly better to HSRL-2 than SPEX with respect to MAE and MRE. It should be noted that the smoke plume exhibits large spatial variation so part of the MAP-lidar differences can be attributed to the fact that different instruments see a slightly different part of the smoke plume. Furthermore, both SPEX and RSP show a similar negative bias in AOD at both 355 nm and 532 nm, and one clear outlier point in the comparison with HSRL-2 at the highest AOD. This is also clear from the corresponding Bland-Altman plots Figs 7e and f. Given the very similar underestimation in both SPEX and RSP (compared to HSRL-2) and the good comparison between SPEX and RSP, it is unlikely that this underestimation is caused by aspects related to instrumental errors of the 2 different MAPs. It might be possible that the underestimation is related to the MAP retrieval approach which is the same for both instruments, but based on earlier studies with real and synthetic measurements we have no indication for this. Another possibility is that HSRL-2 overestimates the AOD at this high aerosol loading or the large spatial variability has a larger effect on the MAP-lidar comparison than on the inter-MAP comparison. At high AOD the performance of RSP is more similar to that of SPEX than for low AOD. Our explanation for this, is that at high AOD the measured radiance and DoLP are less affected by the co-registration errors between viewing angles than for low AOD.

For the high AOD case, we compare also the aerosol depolarization ratio (δ) and aerosol lidar ratio (S) from SPEX and RSP with HSRL-2. Figs 8a-c respectively show the comparison of the aerosol depolarization ratio between SPEX and HSRL-2, between RSP and HSRL-2, and between SPEX and RSP. It can be observed that both SPEX and RSP show a similar behavior against HSRL-2 especially at 355 nm: There is an underestimation towards lower values of depolarization ratio but on the other hand there is a reasonable agreement with HSRL-2 for both instruments. Again, given the fact that the performance of both SPEX and RSP versus HSRL-2 is very similar, we conclude that the main reason for difference between SPEX/RSP and HSRL-2 does not lie in instrumental errors for the MAPs. A possible explanation for the difference could be the simplified description of non-spherical particles in our retrieval approach. On the other hand, the overall comparison of the aerosol depolarization

ratio with HSRL-2 confirms capability of both SPEX and RSP to retrieve information on particle shape. The results of the aerosol lidar ratio are shown in Figs 8d-f. Both SPEX and RSP show a similar overestimation of the lidar ratio compared to HSRL-2, and SPEX and RSP agree quite well. Again, it is unlikely that the overestimation is related to instrumental errors in the MAPs. Overall, the agreement with HSRL-2 for the aerosol lidar ratio is reasonable for both SPEX and RSP.

4.2.4 Median and standard deviation properties of the smoke plume

The median and standard deviation properties for the smoke plume as measured by SPEX and RSP are summarized in Table 3. Here, we only include retrievals for which AOD > 0.2 at 532 nm because for those cases accurate retrieval of microphysical properties is expected (e.g., Hasekamp et al. (2019)). The number of points to calculate the median and the standard deviation is the same for SPEX and RSP. Also, we only include fine mode microphysical properties because there is only a very small coarse mode contribution to the smoke plume. SPEX and RSP compare well for the fine mode refractive index, fine mode effective redius, fine and coarse mode AOD, and SSA (relative to requirements as formulated e.g. by Mishchenko et al. (2004)). Reasonable agreement is found for the fraction of spherical particles. For the Aerosol Layer Height (ALH), SPEX retrieves a higher value (4.417 km) than RSP (1.148 km), where the latter value is somewhat closer to the ALH derived from HSRL-2 (2.64 km). Here, it should be noted that for SPEX the shortest wavelength that is used in the retrieval is 450 nm, so we do not expect an accurate ALH retrieval because the retrieval of ALH from polarization requires a strong signal from Rayleigh scattering (Wu et al., 2016). Figure 9 shows the number particle size distribution from SPEX and RSP in the smoke plume, which confirms the smoke plume is fine mode dominated.

The values of the aerosol properties in Table 3 (for both SPEX and RSP) are in the range that is expected for smoke. First of all, it is expected that smoke is dominated by fine particles (e.g. Russell et al. (2014)), which is confirmed by the much larger retrieved fine mode AOD than coarse mode AOD by both MAPs. The real part of the refractive index is consistent with the study of Levin et al. (2010) for the Fire Laboratory at Missoula Experiment (FLAME), who found mostly refractive indices for biomass burning between 1.55 and 1.60. Also, the SSA values in Table 3 are representative for fresh biomass burning smoke. For example, Nicolae et al. (2013) found SSA values of 0.79 at 532 nm for smoke with an age of 0.25 day and 0.93 for smokes with an age of 0.75 day. Both the values retrieved by SPEX and RSP can be considered realistic for smoke.

5 Discussions and conclusions

In this study, we performed aerosol retrievals from different MAPs employed during the ACEPOL campaign and evaluated them against ground based AERONET measurements and against HSRL-2 measurements. The polarimetric aerosol retrievals were performed using the SRON algorithm in multi-mode setup (Fu and Hasekamp, 2018) on SPEX airborne, RSP (without SWIR channels), and AirMSPI.

For the AERONET comparison, only scenes with low AOD (0.03-0.17 at 440 nm) were available during ACEPOL. For these scenes, SPEX, RSP, and AirMSPI all show good agreement with AERONET for AOD (MAE respectively 0.016, 0.024, and 0.014 for AOD at 440 nm). For the fine mode effective radius, we found MAE with AERONET of 0.022, 0.021, and 0.028

for SPEX, RSP, and AirMSPI, respectively. For the effective radius comparison we only compare scenes with AOD > 0.10 at 380 nm, but it should be noted that the remaining cases are still very challenging and that the difference in performance between the different instruments are caused by just 1 or 2 comparison points. All three instruments had a poor comparison with AERONET for the coarse mode effective radius. This was because the coarse mode effective radius was a difficult parameter to retrieve, in particular for small AOD values. For the fine mode AOD, good agreements with AERONET were shown for all three MAPs with somewhat better performance for AirMSPI. For the coarse mode AOD, SPEX and RSP show reasonable agreement while AirMSPI shows also good agreement here. It should be noted however that the comparison for AirMSPI is not based on exactly the same points as for SPEX and RSP.

For the comparison between the MAPs (SPEX and RSP) and HSRL-2, we focused on a day with low AOD and a flight leg with high AOD (including measurements with AOD > 1.0) over a prescribed forest fire in Arizona (9 November). For the challenging case of low AOD over land, it was shown that SPEX and RSP are capable of providing accurate retrievals of AOD. For this low AOD case, SPEX showed better comparison against HSRL-2 than RSP.

For the retrievals over the smoke plume also a reasonable agreement in AOD between the MAPs and HSRL-2 was found, despite the fact that the comparison was hampered by large spatial variability in AOD throughout the smoke plume. Besides, a good agreement was found between the MAPs (SPEX, RSP) and HSRL-2 for the aerosol depolarization ratio, which indicates MAPs are capable of retrieving particles sphericity. A reasonable comparison was also found for the aerosol lidar ratio.

For the ALH SPEX retrieved a value that was high (by $\sim$1.5 km) compared to HSRL-2 while the ALH retrieved from RSP agreed somewhat better with HSRL-2, although it was $\sim$1 km lower. Here, it should be noted that we do not expect a good ALH retrieval from SPEX airborne, because the shortest wavelength used in the retrieval was 450 nm. For the retrieved microphysical and optical properties of the smoke plume, SPEX and RSP agreed very well with each other and both instruments retrieved smoke properties that were in line with earlier studies.

In this study, 3 polarimeters produced comparable results when using the same algorithm. The exception were the ALH and some coarse mode parameters, which were mainly caused by not having the bands that these parameters were sensitive to: shortwave (410 nm) and SWIR, respectively. For parameters that the instruments were sensitive to, good agreements were found among instruments. Our results corroborate the findings of earlier studies that different combinations of spectral and angular measurements yield a very similar retrieval capability for aerosol properties (Hasekamp and Landgraf, 2007; Wu et al., 2015; Hasekamp et al., 2019)

Data availability. The ACEPOL data from MAPs and lidars can be downloaded from the website: https://www-air.larc.nasa.gov/cgi-bin/ArcView/acepol, (registration required). The AERONET data can be downloaded from the website: https://aeronet.gsfc.nasa.gov/. The meteorological NCEP data can be accessed through the website: http://www.cdc.noaa.gov/. The polarimetric retrieval results will be made available on SRON's ftp site.

Competing interests. The authors declare that no competing interests are present.

Acknowledgements. This work is funded by a NWO/NSO project ACEPOL: Aerosol Characterization from Polarimeter and Lidar under project number ALW-GO/16-09. We thank all the members involved in the ACEPOL campaign. We acknowledge the former Aerosol, Cloud, Ecosystem (ACE) program at NASA's Earth Science Division as a sponsor for ACEPOL flights. We thank the field teams making measurements on the ground as some of those were critical to the measurement accuracy (i.e. vicarious calibration). We also acknowledge the support received by the ground- and aircrew at NASA AFRC in Palmdale and the work performed at the Jet Propulsion Laboratory, California Institute of Technology. We thank the AERONET team and the MERRA-2 team for maintaining the data. NCEP Reanalysis data provided by the NOAA/OAR/ESRL PSD, Boulder, Colorado, USA, from their website at https://www.esrl.noaa.gov/psd/. We would also like to thank the Netherlands Supercomputing Centre (SURFsara) for providing us with the computing facility, the Cartesius cluster. We are very grateful to the editor, Dr Remer, two other reviewers, and Dr Korkin for their reviews and insightful comments.

References

Bottiger, J. R., Fry, E. S., and Thompson, R. C.: Phase Matrix Measurements for Electromagnetic Scattering by Sphere Aggregates, in: Light Scattering by Irregularly Shaped Particles, edited by Schuerman, D. W., pp. 283–290, Springer US, Boston, MA, https://doi.org/10.1007/978-1-4684-3704-1_33, 1980.

Bucholtz, A.: Rayleigh-scattering calculations for the terrestrial atmosphere, Applied Optics, 34, 2765–2773, https://www.osapublishing.org/ao/abstract.cfm?uri=ao-34-15-2765, 1995.

Burton, S. P., Ferrare, R. A., Hostetler, C. A., Hair, J. W., Rogers, R. R., Obland, M. D., Butler, C. F., Cook, A. L., Harper, D. B., and Froyd, K. D.: Aerosol classification using airborne High Spectral Resolution Lidar measurements – methodology and examples, Atmospheric Measurement Techniques, 5, 73–98, https://www.atmos-meas-tech.net/5/73/2012/, 2012.

Burton, S. P., Vaughan, M. A., Ferrare, R. A., and Hostetler, C. A.: Separating mixtures of aerosol types in airborne High Spectral Resolution Lidar data, Atmospheric Measurement Techniques, 7, 419–436, https://www.atmos-meas-tech.net/7/419/2014/amt-7-419-2014.html, 2014.

Burton, S. P., Hair, J. W., Kahnert, M., Ferrare, R. A., Hostetler, C. A., Cook, A. L., Harper, D. B., Berkoff, T. A., Seaman, S. T., Collins, J. E., Fenn, M. A., and Rogers, R. R.: Observations of the spectral dependence of linear particle depolarization ratio of aerosols using NASA Langley airborne High Spectral Resolution Lidar, Atmospheric Chemistry and Physics, 15, 13 453–13 473, https://www.atmos-chem-phys.net/15/13453/2015/, 2015.

Burton, S. P., Hostetler, C. A., Cook, A. L., Hair, J. W., Seaman, S. T., Scola, S., Harper, D. B., Smith, J. A., Fenn, M. A., Ferrare, R. A., Saide, P. E., Chemyakin, E. V., and Müller, D.: Calibration of a high spectral resolution lidar using a Michelson interferometer, with data examples from ORACLES, Applied Optics, 57, 6061–6075, https://www.osapublishing.org/ao/abstract.cfm?uri=ao-57-21-6061, 2018.

Cairns, B., Russell, E. E., and Travis, L. D.: Research Scanning Polarimeter: calibration and ground-based measurements, in: Polarization: Measurement, Analysis, and Remote Sensing II, vol. 3754, pp. 186–197, International Society for Optics and Photonics, https://doi.org/10.1117/12.366329, https://www.spiedigitallibrary.org/conference-proceedings-of-spie/3754/0000/Research-Scanning-Polarimeter-calibration-and-ground-based-measurements/10.1117/12.366329.short, 1999.

Cairns, B., Russell, E. E., LaVeigne, J. D., and Tennant, P. M. W.: Research scanning polarimeter and airborne usage for remote sensing of aerosols, in: Polarization Science and Remote Sensing, vol. 5158, pp. 33–44, International Society for Optics and Photonics, https://www.spiedigitallibrary.org/conference-proceedings-of-spie/5158/0000/Research-scanning-polarimeter-and-airborne-usage-for-remote-sensing-of/10.1117/12.518320.short, 2003.

Cairns, B., LaVeigne, J. D., Rael, A., and Granneman, R. D.: Atmospheric correction of HyperSpecTIR measurements using the research scanning polarimeter, in: Polarization: Measurement, Analysis, and Remote Sensing VI, 12 Apr. 2004, Orlando, Fla., vol. 5432 of *Proc. SPIE*, p. 95, https://doi.org/10.1117/12.542194, 2004.

Chen, C., Dubovik, O., Henze, D. K., Lapyonak, T., Chin, M., Ducos, F., Litvinov, P., Huang, X., and Li, L.: Retrieval of desert dust and carbonaceous aerosol emissions over Africa from POLDER/PARASOL products generated by the GRASP algorithm, Atmospheric Chemistry and Physics, 18, 12 551–12 580, https://www.atmos-chem-phys.net/18/12551/2018/acp-18-12551-2018.html, 2018.

Cheng, T. H., Gu, X. F., Xie, D. H., Li, Z. Q., Yu, T., and Chen, X. F.: Simultaneous retrieval of aerosol optical properties over the Pearl River Delta, China using multi-angular, multi-spectral, and polarized measurements, Remote Sensing of Environment, 115, 1643–1652, https://doi.org/10.1016/j.rse.2011.02.020, 2011.

Chowdhary, J., Cairns, B., Mishchenko, M. I., Hobbs, P. V., Cota, G. F., Redemann, J., Rutledge, K., Holben, B. N., and Russell, E.: Retrieval of Aerosol Scattering and Absorption Properties from Photopolarimetric Observations over the Ocean during the CLAMS Experiment, Journal of the Atmospheric Sciences, 62, 1093–1117, https://doi.org/10.1175/JAS3389.1, 2005.

D'Almeida, G. A., Koepke, P., and Shettle, E. P.: Atmospheric Aerosols: Global Climatology and Radiative Characteristics, A Deepak Pub, Hampton, 1991.

Deschamps, P., Breon, F., Leroy, M., Podaire, A., Bricaud, A., Buriez, J., and Seze, G.: The POLDER mission: instrument characteristics and scientific objectives, IEEE Transactions on Geoscience and Remote Sensing, 32, 598–615, https://doi.org/10.1109/36.297978, 1994.

Deuzé, J. L., Goloub, P., Herman, M., Marchand, A., Perry, G., Susana, S., and Tanré, D.: Estimate of the aerosol properties over the ocean with POLDER, Journal of Geophysical Research: Atmospheres, 105, 15 329–15 346, https://agupubs.onlinelibrary.wiley.com/doi/abs/10.1029/2000JD900148, 2000.

Deuzé, J. L., Goloub, P., Herman, M., Marchand, A., Perry, G., Susana, S., and Tanré, D.: Estimate of the aerosol properties over the ocean with POLDER, J. Geophys. Res., 105, 15+, https://doi.org/10.1029/2000jd900148, 2000.

Deuzé, J. L., Bréon, F. M., Devaux, C., Goloub, P., Herman, M., Lafrance, B., Maignan, F., Marchand, A., Nadal, F., Perry, G., and Tanré, D.: Remote sensing of aerosols over land surfaces from POLDER-ADEOS-1 polarized measurements, Journal of Geophysical Research: Atmospheres, 106, 4913–4926, https://agupubs.onlinelibrary.wiley.com/doi/abs/10.1029/2000JD900364, 2001.

Deuzé, J. L., BréOn, F. M., Devaux, C., Goloub, P., Herman, M., Lafrance, B., Maignan, F., Marchand, A., Nadal, F., Perry, G., and Tanré, D.: Remote sensing of aerosols over land surfaces from POLDER-ADEOS-1 polarized measurements, J. Geophys. Res., 106, 4913–4926, https://doi.org/10.1029/2000jd900364, 2001.

Di Noia, A., Hasekamp, O. P., van Harten, G., Rietjens, J. H. H., Smit, J. M., Snik, F., Henzing, J. S., de Boer, J., Keller, C. U., and Volten, H.: Use of neural networks in ground-based aerosol retrievals from multi-angle spectropolarimetric observations, Atmospheric Measurement Techniques, 8, 281–299, https://www.atmos-meas-tech.net/8/281/2015/, 2015.

Di Noia, A., Hasekamp, O. P., Wu, L., van Diedenhoven, B., Cairns, B., and Yorks, J. E.: Combined neural network/Phillips-Tikhonov approach to aerosol retrievals over land from the NASA Research Scanning Polarimeter, Atmospheric Measurement Techniques, 10, 4235–4252, https://doi.org/10.5194/amt-10-4235-2017, 2017.

Diner, D. J., Xu, F., Garay, M. J., Martonchik, J. V., Rheingans, B. E., Geier, S., Davis, A., Hancock, B. R., Jovanovic, V. M., Bull, M. A., Capraro, K., Chipman, R. A., and McClain, S. C.: The Airborne Multiangle SpectroPolarimetric Imager (AirMSPI): a new tool for aerosol and cloud remote sensing, Atmospheric Measurement Techniques, 6, 2007–2025, https://doi.org/10.5194/amt-6-2007-2013, 2013.

Diner, D. J., Boland, S. W., Brauer, M., Bruegge, C., Burke, K. A., Chipman, R., Girolamo, L. D., Garay, M. J., Hasheminassab, S., Hyer, E., Jerrett, M., Jovanovic, V., Kalashnikova, O. V., Liu, Y., Lyapustin, A. I., Martin, R. V., Nastan, A., Ostro, B. D., Ritz, B., Schwartz, J., Wang, J., and Xu, F.: Advances in multiangle satellite remote sensing of speciated airborne particulate matter and association with adverse health effects: from MISR to MAIA, Journal of Applied Remote Sensing, 12, 042 603, https://www.spiedigitallibrary.org/journals/Journal-of-Applied-Remote-Sensing/volume-12/issue-4/042603/Advances-in-multiangle-satellite-remote-sensing-of-speciated-airborne-particulate/10.1117/1.JRS.12.042603.short, 2018.

Dubovik, O., Holben, B. N., Lapyonok, T., Sinyuk, A., Mishchenko, M. I., Yang, P., and Slutsker, I.: Non-spherical aerosol retrieval method employing light scattering by spheroids, Geophys. Res. Lett., 29, 1415+, https://doi.org/10.1029/2001gl014506, 2002.

Dubovik, O., Sinyuk, A., Lapyonok, T., Holben, B. N., Mishchenko, M., Yang, P., Eck, T. F., Volten, H., Muñoz, O., Veihelmann, B., van der Zande, W. J., Leon, J. F., Sorokin, M., and Slutsker, I.: Application of spheroid models to account for aerosol particle nonsphericity in

remote sensing of desert dust, Journal of Geophysical Research (Atmospheres), 111, D11 208+, https://doi.org/10.1029/2005jd006619, 2006.

Dubovik, O., Herman, M., Holdak, A., Lapyonok, T., Tanré, D., Deuzé, J. L., Ducos, F., Sinyuk, A., and Lopatin, A.: Statistically optimized inversion algorithm for enhanced retrieval of aerosol properties from spectral multi-angle polarimetric satellite observations, Atmospheric Measurement Techniques, 4, 975–1018, https://doi.org/10.5194/amt-4-975-2011, 2011.

Dubovik, O., Li, Z., Mishchenko, M. I., Tanré, D., Karol, Y., Bojkov, B., Cairns, B., Diner, D. J., Espinosa, W. R., Goloub, P., Gu, X., Hasekamp, O., Hong, J., Hou, W., Knobelspiesse, K. D., Landgraf, J., Li, L., Litvinov, P., Liu, Y., Lopatin, A., Marbach, T., Maring, H., Martins, V., Meijer, Y., Milinevsky, G., Mukai, S., Parol, F., Qiao, Y., Remer, L., Rietjens, J., Sano, I., Stammes, P., Stamnes, S., Sun, X., Tabary, P., Travis, L. D., Waquet, F., Xu, F., Yan, C., and Yin, D.: Polarimetric remote sensing of atmospheric aerosols: Instruments, methodologies, results, and perspectives, Journal of Quantitative Spectroscopy and Radiative Transfer, 224, 474–511, http://www.sciencedirect.com/science/article/pii/S0022407318308409, 2019.

Eck, T. F., Holben, B. N., Reid, J. S., Dubovik, O., Smirnov, A., O'Neill, N. T., Slutsker, I., and Kinne, S.: Wavelength dependence of the optical depth of biomass burning, urban, and desert dust aerosols, Journal of Geophysical Research: Atmospheres, 104, 31 333–31 349, https://agupubs.onlinelibrary.wiley.com/doi/abs/10.1029/1999JD900923, 1999.

Fougnie, B., Marbach, T., Lacan, A., Lang, R., Schlüssel, P., Poli, G., Munro, R., and Couto, A. B.: The multi-viewing multi-channel multi-polarisation imager – Overview of the 3MI polarimetric mission for aerosol and cloud characterization, Journal of Quantitative Spectroscopy and Radiative Transfer, 219, 23–32, http://www.sciencedirect.com/science/article/pii/S002240731830373X, 2018.

Fu, G. and Hasekamp, O.: Retrieval of aerosol microphysical and optical properties over land using a multimode approach, Atmospheric Measurement Techniques, 11, 6627–6650, https://doi.org/10.5194/amt-11-6627-2018, 2018.

Gao, M., Zhai, P.-W., Franz, B., Hu, Y., Knobelspiesse, K., Werdell, P. J., Ibrahim, A., Cairns, B., and Chase, A.: Inversion of multi-angular polarimetric measurements over open and coastal ocean waters: a joint retrieval algorithm for aerosol and water leaving radiance properties, Atmospheric Measurement Techniques Discussions, pp. 1–31, https://www.atmos-meas-tech-discuss.net/amt-2019-67/, 2019.

Gelaro, R., McCarty, W., Suárez, M. J., Todling, R., Molod, A., Takacs, L., Randles, C. A., Darmenov, A., Bosilovich, M. G., Reichle, R., Wargan, K., Coy, L., Cullather, R., Draper, C., Akella, S., Buchard, V., Conaty, A., da Silva, A. M., Gu, W., Kim, G.-K., Koster, R., Lucchesi, R., Merkova, D., Nielsen, J. E., Partyka, G., Pawson, S., Putman, W., Rienecker, M., Schubert, S. D., Sienkiewicz, M., and Zhao, B.: The Modern-Era Retrospective Analysis for Research and Applications, Version 2 (MERRA-2), Journal of Climate, 30, 5419–5454, https://journals.ametsoc.org/doi/full/10.1175/JCLI-D-16-0758.1, 2017.

Hair, J. W., Hostetler, C. A., Cook, A. L., Harper, D. B., Ferrare, R. A., Mack, T. L., Welch, W., Izquierdo, L. R., and Hovis, F. E.: Airborne High Spectral Resolution Lidar for profiling aerosol optical properties, Appl. Opt., 47, 6734–6752, http://ao.osa.org/abstract.cfm?URI=ao-47-36-6734, 2008.

Hansen, J. E. and Travis, L. D.: Light scattering in planetary atmospheres, Space Science Reviews, 16, 527–610, https://doi.org/10.1007/BF00168069, https://doi.org/10.1007/BF00168069, 1974.

Hasekamp, O. P.: Capability of multi-viewing-angle photo-polarimetric measurements for the simultaneous retrieval of aerosol and cloud properties, Atmospheric Measurement Techniques, 3, 839–851, https://doi.org/10.5194/amt-3-839-2010, 2010.

Hasekamp, O. P. and Landgraf, J.: A linearized vector radiative transfer model for atmospheric trace gas retrieval, J. Quant. Spec. Radiat. Transf., 75, 221–238, https://doi.org/10.1016/s0022-4073(01)00247-3, 2002.

Hasekamp, O. P. and Landgraf, J.: Retrieval of aerosol properties over the ocean from multispectral single-viewing-angle measurements of intensity and polarization: Retrieval approach, information content, and sensitivity study, J. Geophys. Res., 110, D20 207+, https://doi.org/10.1029/2005jd006212, 2005.

Hasekamp, O. P. and Landgraf, J.: Retrieval of aerosol properties over land surfaces: capabilities of multiple-viewing-angle intensity and polarization measurements, Appl. Opt., 46, 3332–3344, https://doi.org/10.1364/ao.46.003332, 2007.

Hasekamp, O. P., Litvinov, P., and Butz, A.: Aerosol properties over the ocean from PARASOL multiangle photopolarimetric measurements, J. Geophys. Res., 116, D14 204+, https://doi.org/10.1029/2010jd015469, 2011a.

Hasekamp, O. P., Litvinov, P., and Butz, A.: Aerosol properties over the ocean from PARASOL multiangle photopolarimetric measurements, J. Geophys. Res., 116, D14 204+, https://doi.org/10.1029/2010jd015469, 2011b.

Hasekamp, O. P., Fu, G., Rusli, S. P., Wu, L., Di Noia, A., Brugh, J. a. d., Landgraf, J., Martijn Smit, J., Rietjens, J., and van Amerongen, A.: Aerosol measurements by SPEXone on the NASA PACE mission: expected retrieval capabilities, Journal of Quantitative Spectroscopy and Radiative Transfer, 227, 170–184, http://www.sciencedirect.com/science/article/pii/S0022407318308653, 2019.

Herman, M., Deuzé, J. L., Devaux, C., Goloub, P., BréOn, F. M., and Tanré, D.: Remote sensing of aerosols over land surfaces including polarization measurements and application to POLDER measurements, J. Geophys. Res., 102, 17+, https://doi.org/10.1029/96jd02109, 1997.

Hill, S. C., Hill, A. C., and Barber, P. W.: Light scattering by size/shape distributions of soil particles and spheroids, Appl. Opt., 23, 1025–1031, https://doi.org/10.1364/ao.23.001025, 1984.

Holben, B. N., Tanré, D., Smirnov, A., Eck, T. F., Slutsker, I., Abuhassan, N., Newcomb, W. W., Schafer, J. S., Chatenet, B., Lavenu, F., Kaufman, Y. J., Castle, J. V., Setzer, A., Markham, B., Clark, D., Frouin, R., Halthore, R., Karneli, A., O'Neill, N. T., Pietras, C., Pinker, R. T., Voss, K., and Zibordi, G.: An emerging ground-based aerosol climatology: Aerosol optical depth from AERONET, J. Geophys. Res., 106, 12–12 097, https://doi.org/10.1029/2001jd900014, 2001.

Illingworth, A. J., Barker, H. W., Beljaars, A., Ceccaldi, M., Chepfer, H., Clerbaux, N., Cole, J., Delanoë, J., Domenech, C., Donovan, D. P., Fukuda, S., Hirakata, M., Hogan, R. J., Huenerbein, A., Kollias, P., Kubota, T., Nakajima, T., Nakajima, T. Y., Nishizawa, T., Ohno, Y., Okamoto, H., Oki, R., Sato, K., Satoh, M., Shephard, M. W., Velázquez-Blázquez, A., Wandinger, U., Wehr, T., and van Zadelhoff, G.-J.: The EarthCARE Satellite: The Next Step Forward in Global Measurements of Clouds, Aerosols, Precipitation, and Radiation, Bulletin of the American Meteorological Society, 96, 1311–1332, https://journals.ametsoc.org/doi/10.1175/BAMS-D-12-00227.1, 2014.

IPCC: IPCC, 2014: Climate Change 2014: Synthesis Report. Contribution of Working Groups I, II and III to the Fifth Assessment Report of the Intergovernmental Panel on Climate Change [Core Writing Team, R.K. Pachauri and L.A. Meyer (eds.)], Tech. rep., Geneva, Switzerland, https://www.ipcc.ch/report/ar5/syr/, 2014.

Kalnay, E., Kanamitsu, M., Kistler, R., Collins, W., Deaven, D., Gandin, L., Iredell, M., Saha, S., White, G., Woollen, J., Zhu, Y., Leetmaa, A., Reynolds, B., Chelliah, M., Ebisuzaki, W., Higgins, W., Janowiak, J., Mo, K. C., Ropelewski, C., Wang, J., Jenne, R., and Joseph, D.: The NCEP/NCAR 40-Year Reanalysis Project., Bulletin of the American Meteorological Society, 77, 437–472, https://doi.org/10.1175/1520-0477(1996)077%3C0437:tnyrp%3E2.0.co;2, 1996.

Kaufman, Y. and Tanre, D.: Atmospherically resistant vegetation index (ARVI) for EOS-MODIS, IEEE Transactions on Geoscience and Remote Sensing, 30, 261–270, https://doi.org/10.1109/36.134076, 1992.

Knobelspiesse, K., Cairns, B., Mishchenko, M., Chowdhary, J., Tsigaridis, K., van Diedenhoven, B., Martin, W., Ottaviani, M., and Alexandrov, M.: Analysis of fine-mode aerosol retrieval capabilities by different passive remote sensing instrument designs., Optics express, 20, 21 457–21 484, 2012.

Knobelspiesse, K., Tan, Q., Bruegge, C., Cairns, B., Chowdhary, J., Diedenhoven, B. v., Diner, D., Ferrare, R., Harten, G. v., Jovanovic, V., Ottaviani, M., Redemann, J., Seidel, F., and Sinclair, K.: Intercomparison of airborne multi-angle polarimeter observations from the Polarimeter Definition Experiment, Applied Optics, 58, 650–669, https://www.osapublishing.org/ao/abstract.cfm?uri=ao-58-3-650, 2019.

Lacagnina, C., Hasekamp, O. P., Bian, H., Curci, G., Myhre, G., van Noije, T., Schulz, M., Skeie, R. B., Takemura, T., and Zhang, K.: Aerosol single-scattering albedo over the global oceans: Comparing PARASOL retrievals with AERONET, OMI, and AeroCom models estimates, Journal of Geophysical Research (Atmospheres), 120, 9814–9836, https://doi.org/10.1002/2015jd023501, 2015.

Lacagnina, C., Hasekamp, O. P., and Torres, O.: Direct radiative effect of aerosols based on PARASOL and OMI satellite observations, Journal of Geophysical Research (Atmospheres), 122, 2366–2388, https://doi.org/10.1002/2016jd025706, 2017.

Landgraf, J., Hasekamp, O. P., Box, M. A., and Trautmann, T.: A linearized radiative transfer model for ozone profile retrieval using the analytical forward-adjoint perturbation theory approach, J. Geophys. Res., 106, 27+, https://doi.org/10.1029/2001jd000636, 2001.

Lebsock, M. D., L'Ecuyer, T. S., and Stephens, G. L.: Information content of near-infrared spaceborne multiangular polarization measurements for aerosol retrievals, Journal of Geophysical Research: Atmospheres, 112, https://doi.org/10.1029/2007JD008535, 2007.

Levin, E. J. T., McMeeking, G. R., Carrico, C. M., Mack, L. E., Kreidenweis, S. M., Wold, C. E., Moosmüller, H., Arnott, W. P., Hao, W. M., Collett, J. L., and Malm, W. C.: Biomass burning smoke aerosol properties measured during Fire Laboratory at Missoula Experiments (FLAME), Journal of Geophysical Research: Atmospheres, 115, https://agupubs.onlinelibrary.wiley.com/doi/abs/10.1029/2009JD013601, 2010.

Litvinov, P., Hasekamp, O., and Cairns, B.: Models for surface reflection of radiance and polarized radiance: Comparison with airborne multi-angle photopolarimetric measurements and implications for modeling top-of-atmosphere measurements, Remote Sensing of Environment, 115, 781–792, https://doi.org/https://doi.org/10.1016/j.rse.2010.11.005, 2011.

Lopes, F. J. S., Landulfo, E., and Vaughan, M. A.: Evaluating CALIPSO's 532 nm lidar ratio selection algorithm using AERONET sun photometers in Brazil, Atmospheric Measurement Techniques, 6, 3281–3299, https://www.atmos-meas-tech.net/6/3281/2013/, 2013.

Maignan, F., Bréon, F.-M., Fédèle, E., and Bouvier, M.: Polarized reflectances of natural surfaces: Spaceborne measurements and analytical modeling, Remote Sensing of Environment, 113, 2642–2650, https://doi.org/https://doi.org/10.1016/j.rse.2009.07.022, 2009.

Martin Bland, J. and Altman, D.: STATISTICAL METHODS FOR ASSESSING AGREEMENT BETWEEN TWO METHODS OF CLINICAL MEASUREMENT, The Lancet, 327, 307–310, http://www.sciencedirect.com/science/article/pii/S0140673686908378, 1986.

Martins, J. V., Fernandez-Borda, R., McBride, B., Remer, L., and Barbosa, H. M. J.: The Harp Hyperangular Imaging Polarimeter and the Need for Small Satellite Payloads with High Science Payoff for Earth Science Remote Sensing, in: IGARSS 2018 - 2018 IEEE International Geoscience and Remote Sensing Symposium, pp. 6304–6307, https://doi.org/10.1109/IGARSS.2018.8518823, 2018.

Masuda, K., Takashima, T., Kawata, Y., Yamazaki, A., and Sasaki, M.: Retrieval of aerosol optical properties over the ocean using multispectral polarization measurements from space, Applied mathematics and computation, 116, 103–114, https://doi.org/10.1016/S0096-3003(99)00198-8, 2000.

McGill, M., Hlavka, D., Hart, W., Scott, V. S., Spinhirne, J., and Schmid, B.: Cloud Physics Lidar: instrument description and initial measurement results, Appl. Opt., 41, 3725–3734, https://doi.org/10.1364/AO.41.003725, 2002.

Mishchenko, M. I.: Electromagnetic Scattering by Particles and Particle Groups, https://doi.org/10.1017/CBO9781139019064, 2014.

Mishchenko, M. I. and Travis, L. D.: Satellite retrieval of aerosol properties over the ocean using measurements of reflected sunlight: Effect of instrumental errors and aerosol absorption, Journal of Geophysical Research: Atmospheres, 102, 13 543–13 553, https://doi.org/10.1029/97JD01124, 1997.

Mishchenko, M. I., Travis, L. D., Kahn, R. A., and West, R. A.: Modeling phase functions for dust-like tropospheric aerosols using a shape mixture of randomly oriented polydisperse spheroids, J. Geophys. Res., 102, 13 543–13 553, https://doi.org/10.1029/97jd01124, 1997.

Mishchenko, M. I., Cairns, B., Hansen, J. E., Travis, L. D., Burg, R., Kaufman, Y. J., Martins, J. V., and Shettle, E. P.: Monitoring of aerosol forcing of climate from space: analysis of measurement requirements, J. Quant. Spec. Radiat. Transf., 88, 149–161, https://doi.org/10.1016/j.jqsrt.2004.03.030, 2004.

Mishchenko, M. I., Cairns, B., Kopp, G., Schueler, C. F., Fafaul, B. A., Hansen, J. E., Hooker, R. J., Itchkawich, T., Maring, H. B., and Travis, L. D.: Accurate Monitoring of Terrestrial Aerosols and Total Solar Irradiance: Introducing the Glory Mission, Bulletin of the American Meteorological Society, 88, 677–691, https://doi.org/10.1175/bams-88-5-677, 2007.

Mishchenko, M. I., Dlugach, J. M., and Liu, L.: Linear depolarization of lidar returns by aged smoke particles, Appl. Opt., 55, 9968+, https://doi.org/10.1364/ao.55.009968, 2016.

Müller, D., Hostetler, C. A., Ferrare, R. A., Burton, S. P., Chemyakin, E., Kolgotin, A., Hair, J. W., Cook, A. L., Harper, D. B., Rogers, R. R., Hare, R. W., Cleckner, C. S., Obland, M. D., Tomlinson, J., Berg, L. K., and Schmid, B.: Airborne Multiwavelength High Spectral Resolution Lidar (HSRL-2) observations during TCAP 2012: vertical profiles of optical and microphysical properties of a smoke/urban haze plume over the northeastern coast of the US, Atmospheric Measurement Techniques, 7, 3487–3496, https://www.atmos-meas-tech.net/7/3487/2014/, 2014.

Navarro, R.: The NASA Earth Research-2 (ER-2) Aircraft: A Flying Laboratory for Earth Science Studies, Tech. rep., https://ntrs.nasa.gov/search.jsp?R=20070014865, 2007.

Nicolae, D., Nemuc, A., Müller, D., Talianu, C., Vasilescu, J., Belegante, L., and Kolgotin, A.: Characterization of fresh and aged biomass burning events using multiwavelength Raman lidar and mass spectrometry, Journal of Geophysical Research: Atmospheres, 118, 2956–2965, https://agupubs.onlinelibrary.wiley.com/doi/abs/10.1002/jgrd.50324, 2013.

O'Neill, N. T., Eck, T. F., Smirnov, A., Holben, B. N., and Thulasiraman, S.: Spectral discrimination of coarse and fine mode optical depth, Journal of Geophysical Research: Atmospheres, 108, https://agupubs.onlinelibrary.wiley.com/doi/abs/10.1029/2002JD002975, 2003.

Rahman, H., Pinty, B., and Verstraete, M. M.: Coupled surface-atmosphere reflectance (CSAR) model: 2. Semiempirical surface model usable with NOAA advanced very high resolution radiometer data, Journal of Geophysical Research: Atmospheres, 98, 20 791–20 801, https://doi.org/10.1029/93JD02072, https://agupubs.onlinelibrary.wiley.com/doi/abs/10.1029/93JD02072, 1993.

Rogers, R. R., Hair, J. W., Hostetler, C. A., Ferrare, R. A., Obland, M. D., Cook, A. L., Harper, D. B., Burton, S. P., Shinozuka, Y., McNaughton, C. S., Clarke, A. D., Redemann, J., Russell, P. B., Livingston, J. M., and Kleinman, L. I.: NASA LaRC airborne high spectral resolution lidar aerosol measurements during MILAGRO: observations and validation, Atmospheric Chemistry and Physics, 9, 4811–4826, https://www.atmos-chem-phys.net/9/4811/2009/, 2009.

Russell, P. B., Kacenelenbogen, M., Livingston, J. M., Hasekamp, O. P., Burton, S. P., Schuster, G. L., Johnson, M. S., Knobelspiesse, K. D., Redemann, J., Ramachandran, S., and Holben, B.: A multiparameter aerosol classification method and its application to retrievals from spaceborne polarimetry, Journal of Geophysical Research: Atmospheres, 119, 9838–9863, https://agupubs.onlinelibrary.wiley.com/doi/abs/10.1002/2013JD021411, 2014.

Sano, I., Nishina, M., Nakashima, O., Okada, Y., and Mukai, S.: Aerosol retrieval based on combination use of multi-sensor data, in: 36th COSPAR Scientific Assembly, vol. 36 of *COSPAR Meeting*, http://adsabs.harvard.edu/cgi-bin/nph-bib_query?bibcode=2006cosp...36.3884S, 2006.

Schepers, D., aan de Brugh, J. M. J., Hahne, P., Butz, A., Hasekamp, O. P., and Landgraf, J.: LINTRAN v2.0: A linearised vector radiative transfer model for efficient simulation of satellite-born nadir-viewing reflection measurements of cloudy atmospheres, Journal of

Quantitative Spectroscopy and Radiative Transfer, 149, 347–359, http://www.sciencedirect.com/science/article/pii/S002240731400363X, 2014.

Smit, J. M., Rietjens, J. H. H., Harten, G. v., Noia, A. D., Laauwen, W., Rheingans, B. E., Diner, D. J., Cairns, B., Wasilewski, A., Knobelspiesse, K. D., Ferrare, R., and Hasekamp, O. P.: SPEX airborne spectropolarimeter calibration and performance, Applied Optics, 58, 5695–5719, https://www.osapublishing.org/ao/abstract.cfm?uri=ao-58-21-5695, 2019.

Snik, F., Karalidi, T., and Keller, C. U.: Spectral modulation for full linear polarimetry, Appl. Opt., 48, 1337–1346, https://doi.org/10.1364/AO.48.001337, 2009.

Stamnes, S., Hostetler, C., Ferrare, R., Burton, S., Liu, X., Hair, J., Hu, Y., Wasilewski, A., Martin, W., Diedenhoven, B. V., Chowdhary, J., Cetinić, I., Berg, L. K., Stamnes, K., and Cairns, B.: Simultaneous polarimeter retrievals of microphysical aerosol and ocean color parameters from the "MAPP" algorithm with comparison to high-spectral-resolution lidar aerosol and ocean products, Appl. Opt., 57, https://doi.org/10.1364/ao.57.002394, 2018.

Stap, F. A., Hasekamp, O. P., and Röckmann, T.: Sensitivity of PARASOL multi-angle photopolarimetric aerosol retrievals to cloud contamination, Atmospheric Measurement Techniques, 8, 1287–1301, http://dx.doi.org/10.5194/amt-8-1287-2015, 2015.

Stap, F. A., Hasekamp, O. P., Emde, C., and Röckmann, T.: Multiangle photopolarimetric aerosol retrievals in the vicinity of clouds: Synthetic study based on a large eddy simulation, Journal of Geophysical Research: Atmospheres, 121, https://doi.org/10.1002/2016JD024787, 2016.

van Harten, G., de Boer, J., Rietjens, J. H. H., Di Noia, A., Snik, F., Volten, H., Smit, J. M., Hasekamp, O. P., Henzing, J. S., and Keller, C. U.: Atmospheric aerosol characterization with a ground-based SPEX spectropolarimetric instrument, Atmospheric Measurement Techniques, 7, 4341–4351, https://www.atmos-meas-tech.net/7/4341/2014/, 2014.

Waquet, F., Cairns, B., Knobelspiesse, K., Chowdhary, J., Travis, L. D., Schmid, B., and Mishchenko, M. I.: Polarimetric remote sensing of aerosols over land, Journal of Geophysical Research (Atmospheres), 114, D01 206+, https://doi.org/10.1029/2008jd010619, 2009.

Waquet, F., Péré, J. C., Peers, F., Goloub, P., Ducos, F., Thieuleux, F., and Tanré, D.: Global detection of absorbing aerosols over the ocean in the red and near-infrared spectral region, Journal of Geophysical Research: Atmospheres, 121, https://doi.org/10.1002/2016JD025163, 2016.

Werdell, P. J., Behrenfeld, M. J., Bontempi, P. S., Boss, E., Cairns, B., Davis, G. T., Franz, B. A., Gliese, U. B., Gorman, E. T., Hasekamp, O., Knobelspiesse, K. D., Mannino, A., Martins, J. V., McClain, C. R., Meister, G., and Remer, L. A.: The Plankton, Aerosol, Cloud, ocean Ecosystem (PACE) mission: Status, science, advances, Bulletin of the American Meteorological Society, https://journals.ametsoc.org/doi/abs/10.1175/BAMS-D-18-0056.1, 2019.

Winker, D. M., Pelon, J., Coakley, J. A., Ackerman, S. A., Charlson, R. J., Colarco, P. R., Flamant, P., Fu, Q., Hoff, R. M., Kittaka, C., Kubar, T. L., Le Treut, H., Mccormick, M. P., Mégie, G., Poole, L., Powell, K., Trepte, C., Vaughan, M. A., and Wielicki, B. A.: The CALIPSO Mission, Bulletin of the American Meteorological Society, 91, 1211–1230, https://doi.org/10.1175/2010BAMS3009.1, 2010.

Wu, L., Hasekamp, O., van Diedenhoven, B., and Cairns, B.: Aerosol retrieval from multiangle, multispectral photopolarimetric measurements: importance of spectral range and angular resolution, Atmospheric Measurement Techniques, 8, 2625–2638, https://doi.org/10.5194/amt-8-2625-2015, 2015.

Wu, L., Hasekamp, O., van Diedenhoven, B., Cairns, B., Yorks, J. E., and Chowdhary, J.: Passive remote sensing of aerosol layer height using near-UV multiangle polarization measurements, Geophys. Res. Lett., 43, 8783–8790, https://doi.org/10.1002/2016gl069848, 2016.

Wyzga, R. E. and Rohr, A. C.: Long-term particulate matter exposure: Attributing health effects to individual PM components, Journal of the Air & Waste Management Association, 65, 523–543, https://doi.org/10.1080/10962247.2015.1020396, 2015.

Xu, F., van Harten, G., Diner, D. J., Kalashnikova, O. V., Seidel, F. C., Bruegge, C. J., and Dubovik, O.: Coupled retrieval of aerosol properties and land surface reflection using the Airborne Multiangle SpectroPolarimetric Imager, Journal of Geophysical Research (Atmospheres), 122, 7004–7026, https://doi.org/10.1002/2017jd026776, 2017.

Xu, F., Harten, G. v., Diner, D. J., Davis, A. B., Seidel, F. C., Rheingans, B., Tosca, M., Alexandrov, M. D., Cairns, B., Ferrare, R. A., Burton, S. P., Fenn, M. A., Hostetler, C. A., Wood, R., and Redemann, J.: Coupled Retrieval of Liquid Water Cloud and Above-Cloud Aerosol Properties Using the Airborne Multiangle SpectroPolarimetric Imager (AirMSPI), Journal of Geophysical Research: Atmospheres, 123, 3175–3204, https://agupubs.onlinelibrary.wiley.com/doi/abs/10.1002/2017JD027926, 2018.

Xu, F., Diner, D. J., Dubovik, O., and Schechner, Y.: A Correlated Multi-Pixel Inversion Approach for Aerosol Remote Sensing, Remote Sensing, 11, 746, https://www.mdpi.com/2072-4292/11/7/746, 2019.

Yorks, J. E., McGill, M. J., Scott, V. S., Wake, S. W., Kupchock, A., Hlavka, D. L., Hart, W. D., and Selmer, P. A.: The Airborne Cloud–Aerosol Transport System: Overview and Description of the Instrument and Retrieval Algorithms, Journal of Atmospheric and Oceanic Technology, 31, 2482–2497, https://journals.ametsoc.org/doi/full/10.1175/JTECH-D-14-00044.1, 2014.

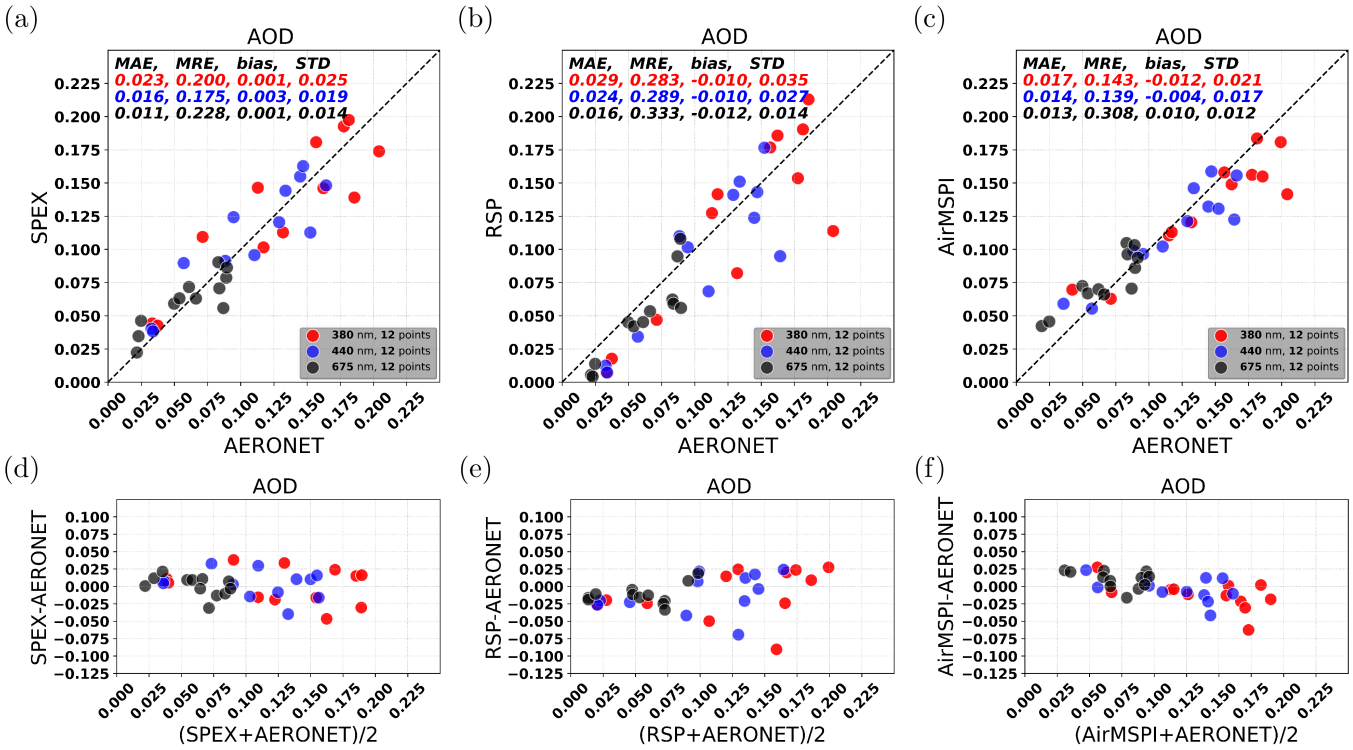

Figure 1. Comparison with AERONET for AOD (380 nm, 440 nm and 675 nm) among SPEX, RSP, and AirMSPI retrievals. **(a)**,**(b)**,**(c)** SPEX, RSP, and AirMSPI comparison with AERONET respectively. **(d)**,**(e)**,**(f)** Bland-Altman plots (or difference plots) between SPEX and AERONET, between RSP and AERONET, and between AirMSPI and AERONET, respectively.

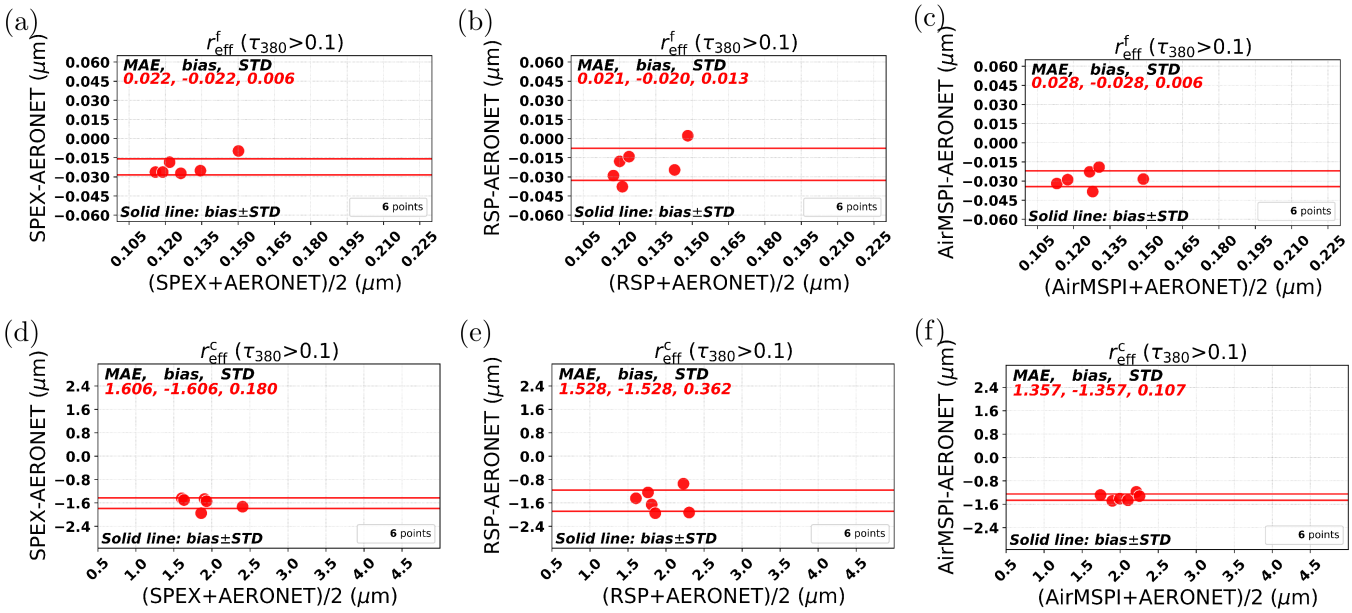

Figure 2. Comparison with AERONET for the effective radius of the fine and coarse modes (r^{f}_{eff} and r^{c}_{eff}), among SPEX, RSP, and AirMSPI retrievals. (a),(b),(c) Bland-Altman plots for r^{f}_{eff} between SPEX and AERONET, between RSP and AERONET, and between AirMSPI and AERONET, respectively. **(d),(e),(f)** Bland-Altman plots for r^{c}_{eff} between SPEX and AERONET, between RSP and AERONET, and between AirMSPI and AERONET, respectively.

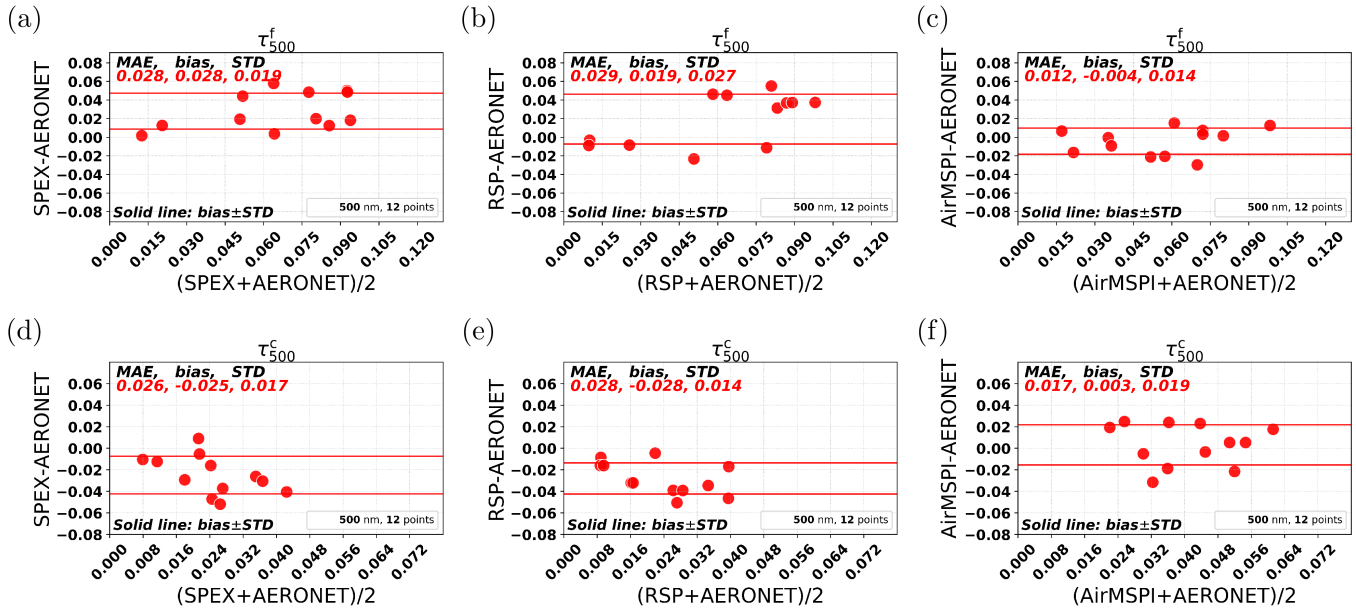

Figure 3. Comparison with AERONET for the AOD of the fine and coarse modes (τ^{f}_{500} and τ^{c}_{500}) among SPEX, RSP, and AirMSPI retrievals. (a),(b),(c) Bland-Altman plots for τ^{f}_{500} between SPEX and AERONET, between RSP and AERONET, and between AirMSPI and AERONET, respectively. **(d),(e),(f)** Bland-Altman plots for τ^{c}_{500} between SPEX and AERONET, between RSP and AERONET, and between AirMSPI and AERONET, respectively.

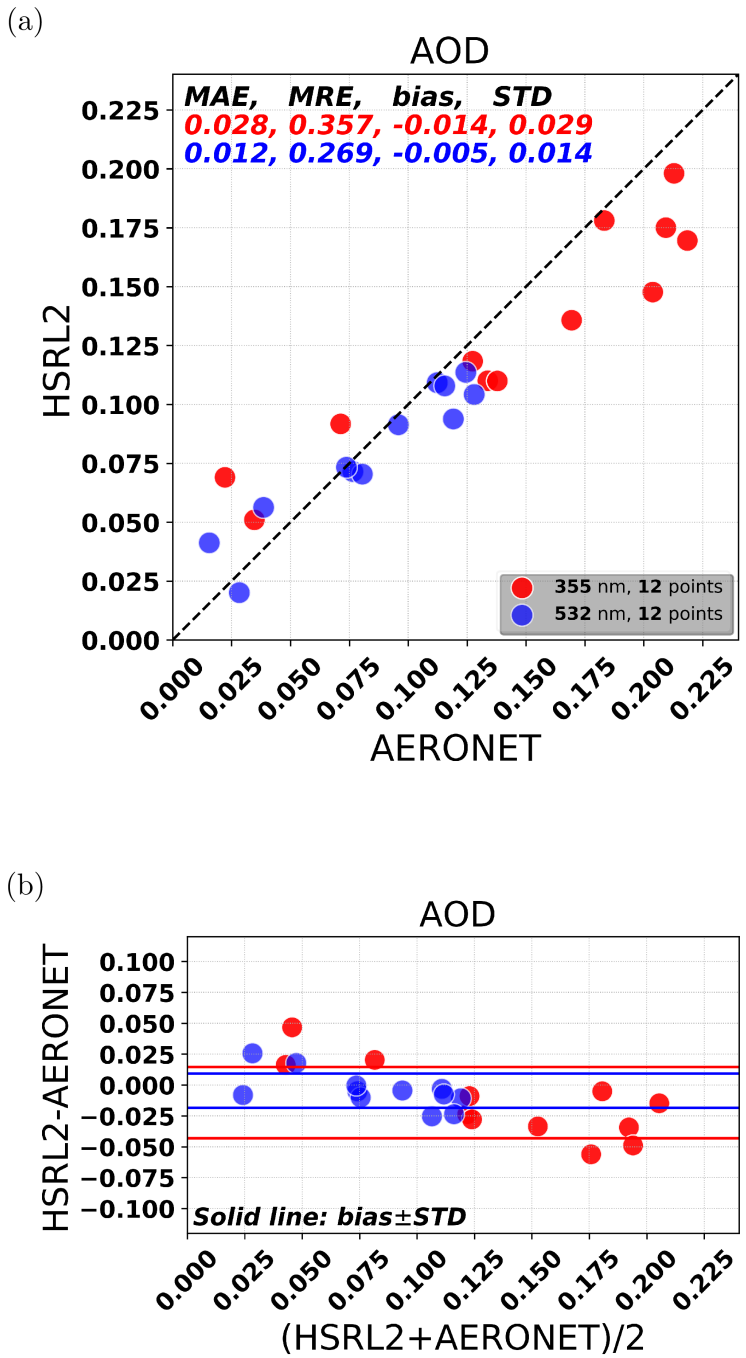

Figure 4. Comparison between HSRL-2 and AERONET for AOD at 355 nm and 532 nm. **(a)** and **(b)** are the scatter plot and the difference plot, respectively.

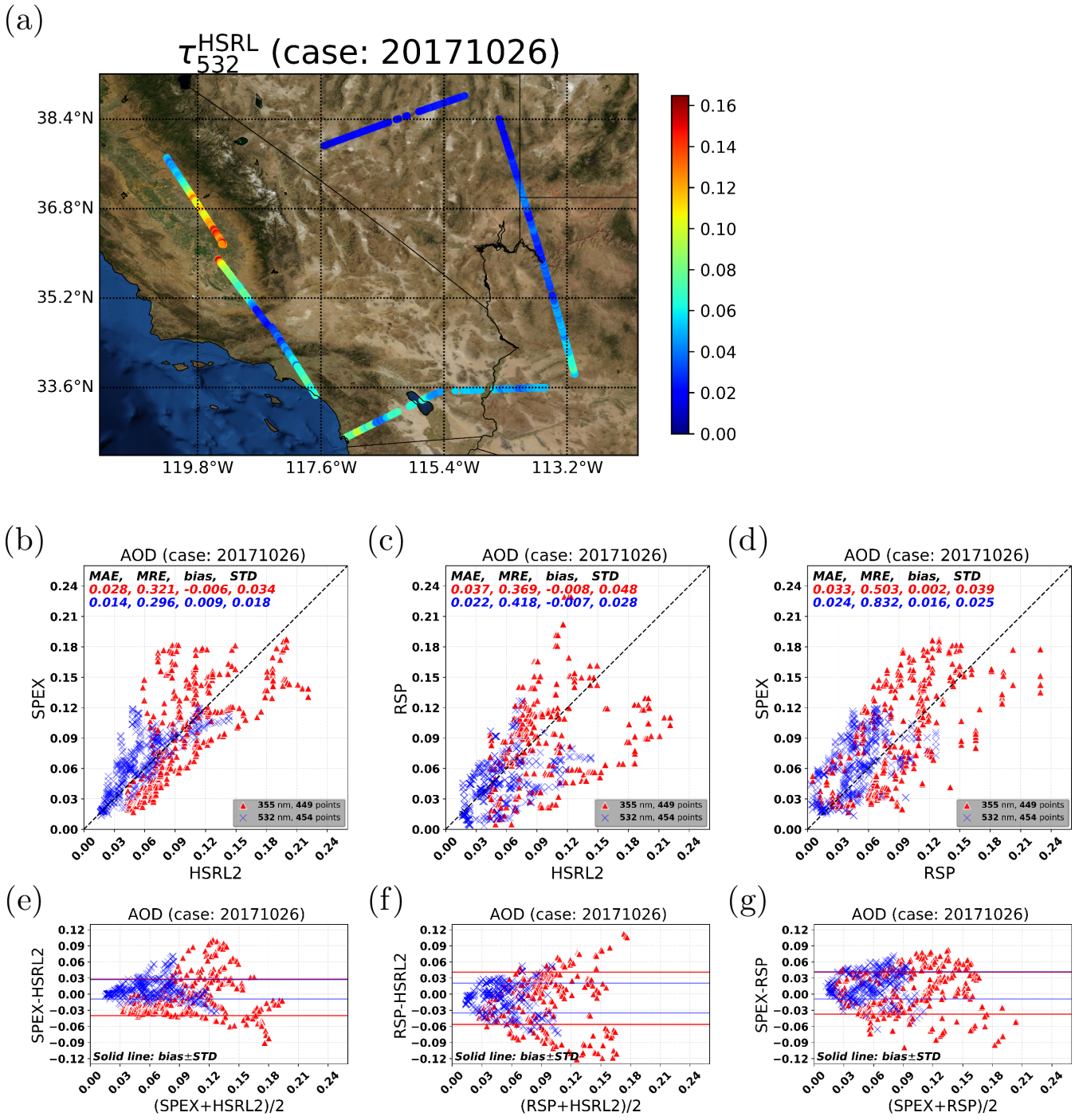

Figure 5. Comparison with HSRL-2 from 26 Oct 2017 (low AOD case) for AOD (355 nm and 532 nm) between SPEX and RSP retrievals. (a) HSRL-2 AOD colocation with SPEX and RSP. (The map is generated using python's basemap package and its arcgis image service 'ESRI_Imagery_World_2D'.) **(b)** SPEX AOD comparison with HSRL-2. **(c)** RSP AOD comparison with HSRL-2. **(d)** SPEX AOD comparison with RSP. **(e)**,**(f)**,**(g)** Bland-Altman plots for **(b)**,**(c)**,**(d)**, respectively.

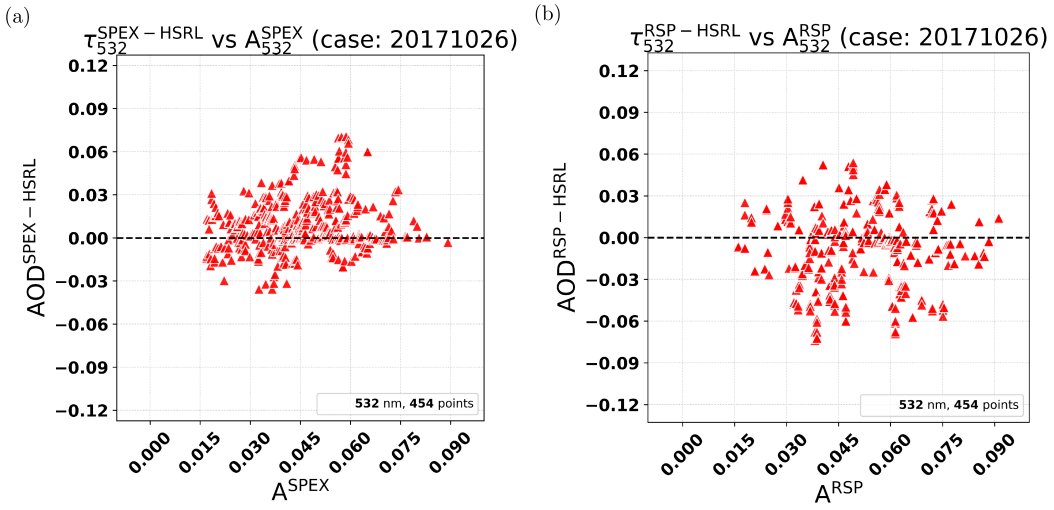

Figure 6. The AOD difference between MAP and HSRL-2 as function of retrieved BRDF scaling parameter A at 532 nm. (a) AOD difference between SPEX and HSRL-2 versus A. **(b)** AOD difference between RSP and HSRL-2 versus A.

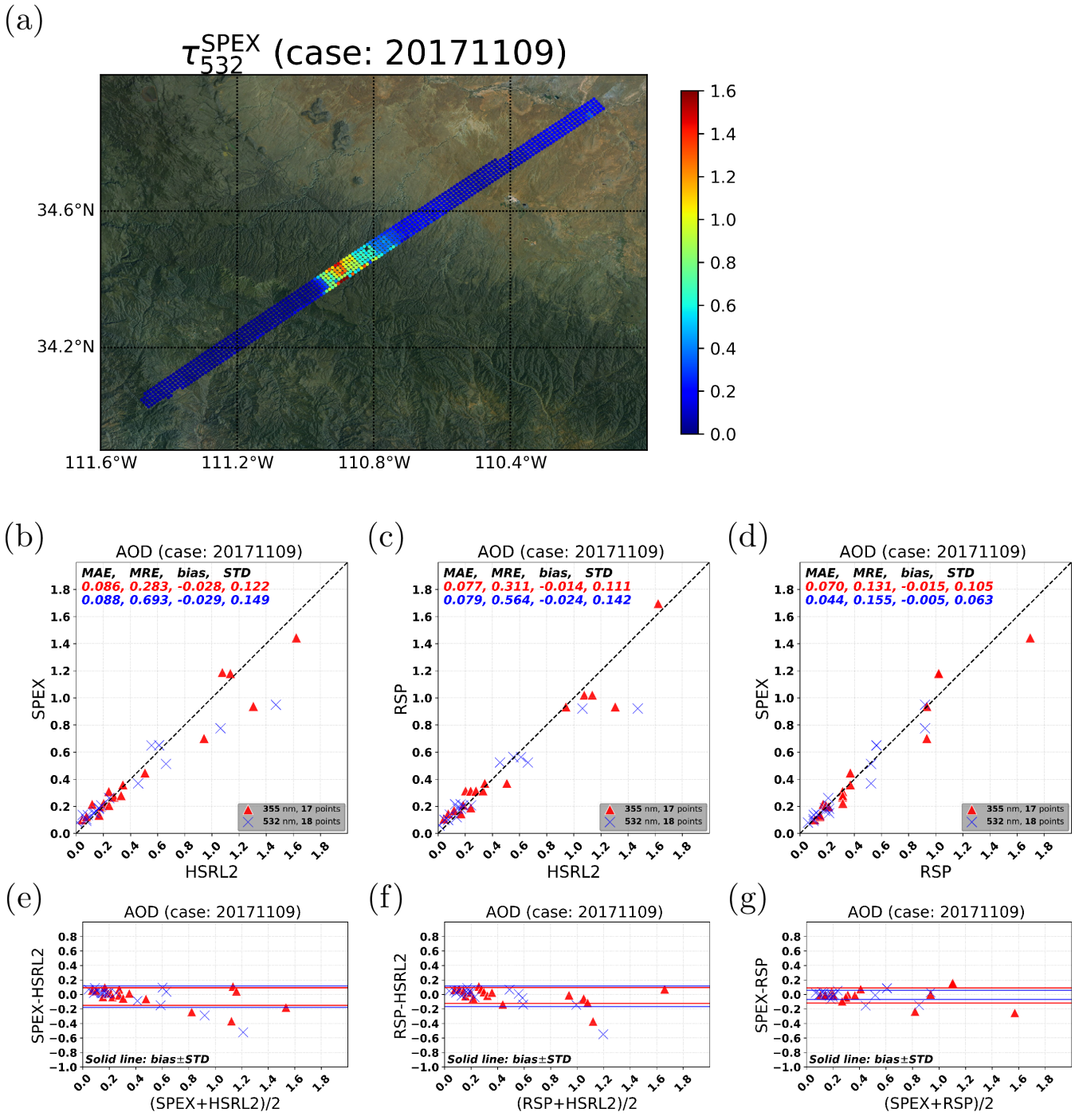

Figure 7. Comparison with HSRL-2 from 9 Nov 2017 (high AOD smoke case) for AOD (355 nm and 532 nm) between SPEX and RSP retrievals. **(a)** SPEX original AOD, i.e., no filter or colocation included. (The map is generated using python's basemap package and its arcgis image service 'ESRI_Imagery_World_2D'.) **(b)** SPEX AOD comparison with HSRL-2. **(c)** RSP AOD comparison with HSRL-2. **(d)** SPEX AOD comparison with RSP. **(e)**,**(f)**,**(g)** Bland-Altman plots for **(b)**,**(c)**,**(d)**, respectively.

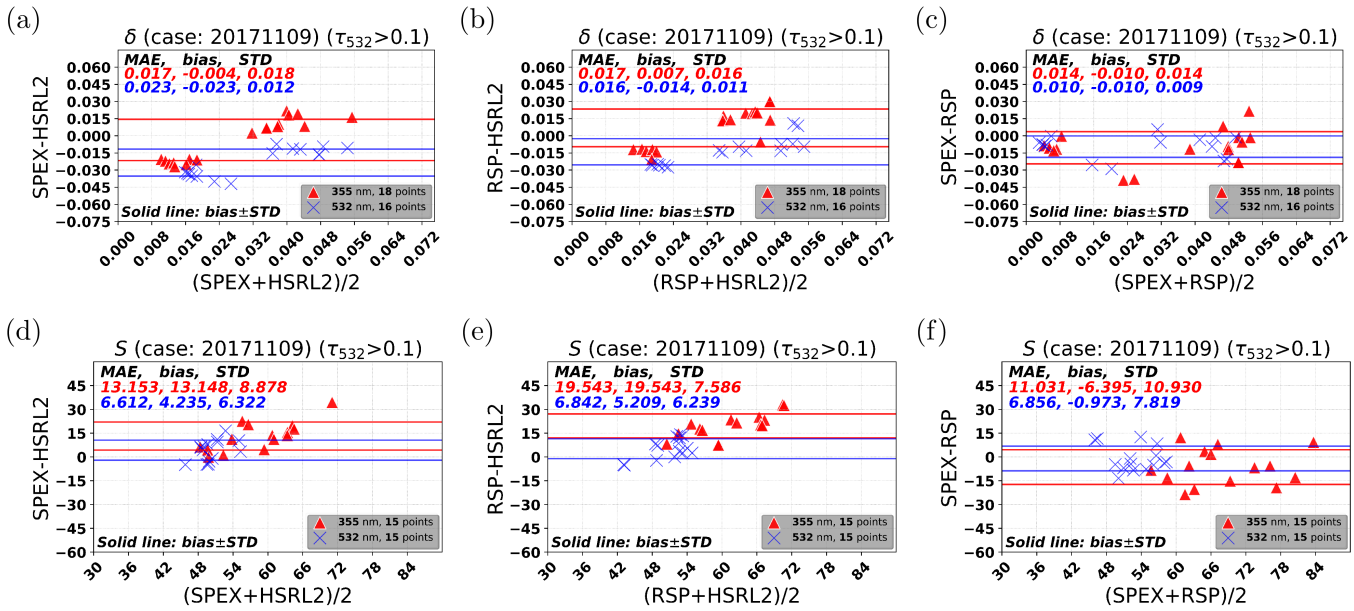

Figure 8. Comparison with HSRL-2 from 9 Nov 2017 (high AOD smoke case) for the aerosol depolarization ratio (δ) and the aerosol lidar ratio (S) between SPEX and RSP retrievals. (a) SPEX δ comparison with HSRL-2. **(b)** RSP δ comparison with HSRL-2. **(c)** SPEX δ comparison with RSP. **(d)** SPEX S comparison with HSRL-2. **(e)** RSP S comparison with HSRL-2. **(f)** SPEX S comparison with RSP.

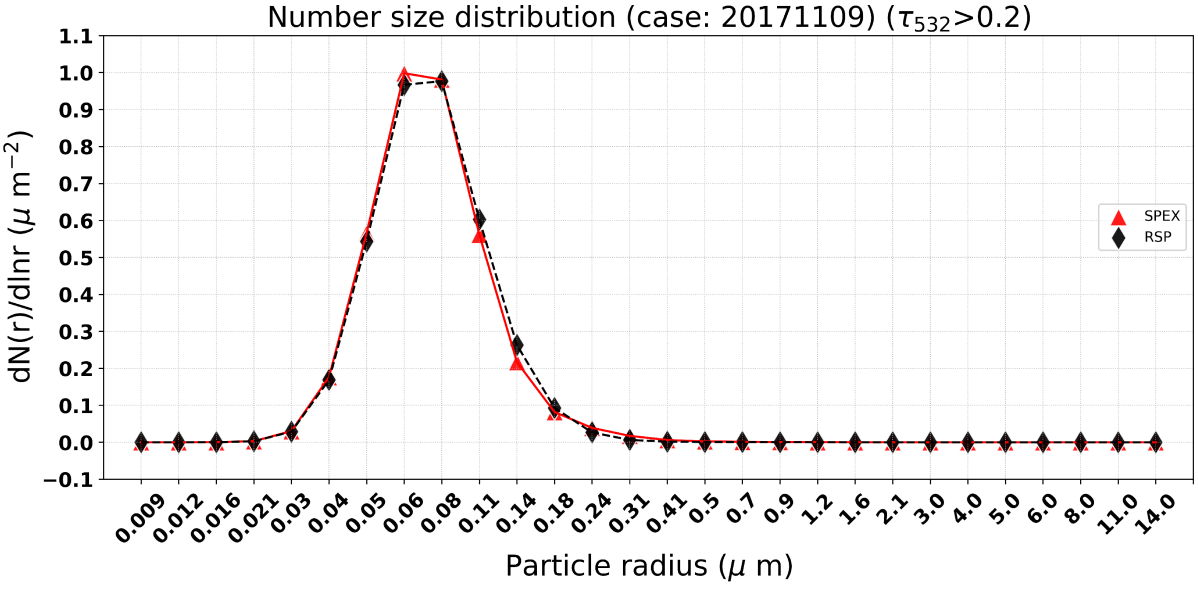

Figure 9. Number particle size distribution in the smoke plume retrieved from SPEX and RSP.

Table 1. Definition of the effective radius (r_{eff}) and the effective variance (v_{eff}) in the SRON 5-mode retrieval.

	Mode 1	Mode 2	Mode 3	Mode 4	Mode 5
r_{eff} (μm)	0.094	0.163	0.282	0.882	1.759
v_{eff}	0.130	0.130	0.130	0.284	1.718

Table 2. Viewing angles and wavelengths used in retrievals among SPEX airborne, RSP, and AirMSPI, and the retrieved parameters from them. Prior values and weighting factors for the state vector are also listed in the table. In this paper, 5-mode retrieval is used, thus $n_{\mathrm{mode}} = 5$. The arrow "$\rightarrow$", "$\leftarrow$", or "$\uparrow$" means the same value with the arrow direction. The prior value and weighting factor of aerosol loading for each mode are calculated based on Mie theory using the prior information of AOD from the table (listed in the row of aerosol loading).

	Polarimeters	SPEX airborne	RSP	AirMSPI		
	Viewing angles	$\pm 56^\circ$, $\pm 42^\circ$, $\pm 28^\circ$, $\pm 14^\circ$, and 0° ($n_{\mathrm{vza}}^{\mathrm{spex}} = 9$)	Averaged based on ~150 angles ($n_{\mathrm{vza}}^{\mathrm{rsp}} = 10$)	$\pm 66^\circ$, $\pm 59^\circ$, $\pm 48^\circ$, $\pm 29^\circ$, and 0° ($n_{\mathrm{vza}}^{\mathrm{airmspi}} = 9$) in step-and-stare mode		
	Wavelengths (radiance)	450, 460, 470, 480, 490, 500, 510, 520, 530, 540, 550, 565, 580, 600, 670, and 750 nm ($n_{\mathrm{wave}}^{\mathrm{spex}} = 16$)	410, 469.1, 554.9, 670, and 863.4 nm ($n_{\mathrm{wave}}^{\mathrm{rsp}} = 5$)	355, 380, 445, 470, 555, 660, and 865 nm ($n_{\mathrm{wave}}^{\mathrm{airmspi}} = 7$)		
	Wavelengths (polarization)	$\uparrow$	$\uparrow$	470, 660, and 865 nm		
					Prior	Weight
Retrieved Aerosol properties	Aerosol loading for each mode	$\rightarrow$	N^j, $(j = 1, 2, ..., n_{\mathrm{mode}})$	$\leftarrow$	0.0001	$(\frac{0.25}{n_{\mathrm{mode}}})^2$
	Fraction of spheres	$\rightarrow$	$f_{\mathrm{sphere}}^{\mathrm{c}}$	$\leftarrow$	0.5	0.25
	Fine mode component coefficient 1 (INORG)	$\rightarrow$	α_1^{f}	$\leftarrow$	0.95	0.1^2
	Fine mode component coefficient 2 (BC)	$\rightarrow$	α_2^{f}	$\leftarrow$	0.005	0.1^2
	Coarse mode component coefficient 1 (INORG)	$\rightarrow$	α_1^{c}	$\leftarrow$	0.95	0.1^2
	Coarse mode component coefficient 2 (DUST)	$\rightarrow$	α_2^{c}	$\leftarrow$	0.005	0.1^2
	Aerosol layer height (km)	$\rightarrow$	ALH	$\leftarrow$	2.0	4.0^2
Retrieved Surface properties	BRDF scaling parameters for wavelength bands	$A(1, 2, \cdots, n_{\mathrm{wave}}^{\mathrm{spex}})$	$A(1, 2, \cdots, n_{\mathrm{wave}}^{\mathrm{rsp}})$	$A(1, 2, \cdots, n_{\mathrm{wave}}^{\mathrm{airmspi}})$	0.0	0.5^2
	Parameter 1 of RPV model	$\rightarrow$	g	$\leftarrow$	-0.09	0.5^2
	Parameter 2 of RPV model	$\rightarrow$	k	$\leftarrow$	0.80	0.5^2
	Scaling parameter for polarized reflectance	$\rightarrow$	B	$\leftarrow$	4.0	2.0^2

Table 3. Median and standard deviation (STD) properties of the smoke plume from SPEX and RSP when AOD > 0.2 at 532 nm.

	SPEX		RSP	
	Median	STD	Median	STD
Fine mode real part of refractive index ($m^{\mathrm{f}}_{\mathrm{r},532}$)	1.579	0.019	1.556	0.059
Fine mode imaginary part of refractive index ($m^{\mathrm{f}}_{\mathrm{i},532}$)	0.038	0.011	0.036	0.013
Fine mode effective radius ($r^{\mathrm{f}}_{\mathrm{eff}}$)	0.116	0.004	0.119	0.007
Fine mode AOD (τ^{f}_{532})	0.554	0.238	0.509	0.231
Coarse mode AOD (τ^{c}_{532})	0.016	0.011	0.040	0.029
Aerosol layer height (ALH) (km)	4.417	1.148	1.585	1.588
SSA (ω_{532})	0.815	0.044	0.829	0.044
Fraction of spherical particles (f_{sphere})	0.989	0.149	0.846	0.133